Chapter 3

Catalytic Reduction of Nitrophenols using NanoSilver Supported on SPAC, PSAC, PCAC and PAC

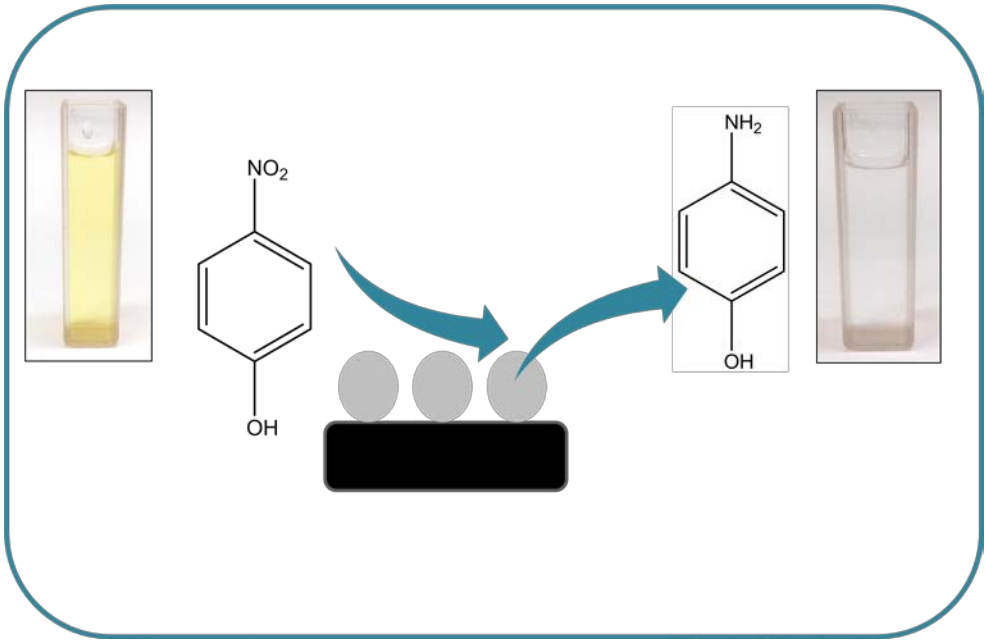

3.1 Introduction

The most amenable method for removal of Nitrophenols is by treatment with a catalyst which reduces it into 4-Aminophenol (4-AP) (Murugan and Jebaranjitham, 2012). This method of remediation for nitroaromatic compounds has gained interest (Cárdenas-Lizana et al., 2012; Coccia et al., 2012; Li J. et al., 2012; Zarejousheghani et al., 2013; Zhang J. et al., 2013; Zhang P. et al., 2011) as it is a green process avoiding the use of organic solvents. Further the products, aromatic amines are widely used as intermediates for the synthesis of dyes, pharmaceuticals, and agrochemicals (Ishida and Haruta, 2007; Kleist et al., 2009; Liu et al., 2010; Rajagopal and Spatola, 1995).

However, the traditional methods for reduction of such nitro compounds involve the use of reagents such as Raney Ni in the presence of acid (Crossley, 1922; Nadagouda et al., 2011). The process is thus not green, but costly and environmentally hazardous. A cleaner alternative is employing $NaBH_4$ in water as the hydride source; but reduction of nitro groups with $NaBH_4$ in the absence of any catalyst is time consuming. Many different metals including Au, Ag, Pt and Pd have been used as catalysts for this purpose (Dotzauer et al., 2009; Li X. et al., 2012; Mei et al., 2005; Rajesh and Venkatesan, 2012).

During reduction catalyzed by Ag, it was observed that smaller Agnps usually showed higher activity, due to a more favorable negative redox potential and higher surface-to volume ratio which facilitated electron transfer from surface of Agnps to reactants (Mori et al., 2009; Zhang et al., 2012). However, the use of small-sized Agnps as catalysts resulted in their aggregation thus minimizing the surface area of catalysts (Cañamares et al., 2005; Hu et al., 2015). Dispersion of Agnps in colloidal form was adopted to overcome this drawback (Yang et al., 2013; Zhang and Yu, 2014). However, this resulted in passivation of some surface-active sites of Agnps and hence reduced catalytic activities. Further, the highly dispersed Agnps were also difficult to separate and recycle (Patel et al., 2007; Zhang Z. et al., 2011).

A feasible solution to overcome these drawbacks was immobilization of Agnps onto a support so as to retain both the high catalytic activity and reusability of the catalysts (Liu et al., 2015; Mao et al., 2015; Zhu et al., 2013).

In order to control their catalytic properties, the catalytically active metal nps have also been immobilized on solid supports with mesopores such as SBA-15 (Zhang X.

et al., 2013; Zheng et al., 2013) and MCM- 41 (Chen et al., 2013; Selvakannan et al., 2013; Venezia et al., 2010) which have been regarded as ideal supports for heterogeneous catalysis due to their excellent stability, high surface area, tunable pore size, and robust surface chemistry. Naik et al. have reported the formation of Agnp within the pores of mesoporous silicas (e.g., SBA-15, MCM-41) and mesoporous γ-alumina and applied the materials as catalysts for the reduction of 4-NP to 4-AP (Naik B. et al., 2011; Naik B. et al., 2012).

Other supports include silica (Chen et al., 2005), silica nanotubes (Zhang Y. et al., 2011), Al_2O_3 (Liu et al., 2013; Patil et al., 2004; Peláez et al., 2013; Shimizu et al., 2011), halloysite (Liu and Zhao, 2009), TiO_2 (Chusuei et al., 2000), zeolites (Patterson et al., 2007), carbon nanotubes (Fortunati et al., 2011; Guo and Li, 2005), graphene oxide (Sreekanth et al., 2016), polyamino cyclodextrin (Russo et al., 2015), polymers (Xiong et al., 2012), polymer resins (Kuroda et al., 2009) and inorganic spheres (Chen et al., 2005; Shin et al., 2009). Leelavathi et al., used quantum clusters of silver supported SiO_2, TiO_2, Fe_2O_3 and Al_2O_3 as catalysts for reduction of nitro compounds (Leelavathi et al., 2011). Dong et al. fabricated a fibrous nano-silica (KCC-1) based nanocatalyst (Ag/KCC-1) for the reduction of 4-NP and 2-nitroaniline using aqueous solution of $NaBH_4$ at room temperature(Dong et al., 2014). Liu et al. fabricated an Ag NPs/Si chip using porous Si and investigated its catalytic potential towards reduction of nitro aromatics (Liu et al., 2014). Shimizu et al. found that silver clusters supported on Al_2O_3 exhibited highly chemo selective reductive activity on the nitro group for the reduction of substituted nitroaromatics (Shimizu et al., 2010). "Cooperation of the acid-base pair sites on Al_2O_3 and the coordinatively unsaturated Ag sites on the silver clusters" were reported to be responsible for the rate-limiting H_2 dissociation to yield an H^+/H^- pair at the metal/support interface, while the basic site on Al_2O_3 acts as an adsorption site for the nitro aromatics.

The formation of Agnps on biological matrices has also been paid particular attention in catalytic applications. Jia et al. used a solid biological organic matrix derived from cuttlebone as scaffold and reducer for the formation of Agnps; the resulting composite was further utilized as catalyst for the reduction of 4-nitrophenol (Jia et al., 2008). Chitosan and calcium alginate have also been used (Murugadoss and Chattopadhyay, 2008; Saha et al., 2010). Bhui and Mishra synthesized worm like Ag nanostructures in methyl cellulose matrix as an efficient catalyst for the reduction of 4-NP to AP by $NaBH_4$ (Bhui and Misra, 2012). Rajesh et al. have synthesized nanocatalysts based on

Agnps encapsulated on three generations of PAMAM dendrimers with varying chain branches that have been grafted on graphite surface (Rajesh and Venkatesan, 2012). Gao et al. utilized Agnps supported onto electrospun polyacrylonitrile micro fibres for catalytic reduction of 4-NP. SPR-induced ultrafast thermal effect and $NaBH_4$ as the electron donor was attributed to the enhanced catalytic activity of Ag/PAN composite fibrous networks effect (Gao et al., 2016).

The fabrication of polymeric composite materials and other composites consisting of Ag has attracted much attention recently (Esumi et al., 2004; Liang et al., 2007; Mallick et al., 2004; Mbhele et al., 2003; Murugan and Jebaranjitham, 2012; Zhang and Han, 2003). Manivannan et al. synthesised a silicate and β-CD composite nanocatalyst for the reduction of 4-NP (Manivannan et al., 2012). Chi et al. have synthesized Fe_3O_4@SiO_2-Ag magnetic nanocomposite based nps for catalytic reduction of 4-NP (Chi et al., 2012). The catalytic activity of the Ag/HZSM-5 nano composite was investigated for the reduction of 4-NP, Congo-red, RhodamineB and methylene blue using aqueous solution of $NaBH_4$ at room temperature (Tajbakhsh et al., 2016). Nasrollahzadeh et al. synthesized Ag/Reduced Graphene Oxide/TiO_2 nanocomposite through a green method using *Euphorbia helioscopia* L. leaf extract as a stabilizing and reducing agent and investigated the reduction of 4-NP, congo red and methylene blue (Nasrollahzadeh et al., 2016).

However, very little effort has been directed towards the preparation of metal catalysts supported on carbonaceous materials and the application of carbon supported Ag catalysts in hydrogen mediated reactions. Carbon offers a number of advantages over oxide and other supports, in being cost effective, stable in acid and base media and the possibility of tuning porosity, specific surface area and surface chemistry for specific catalytic applications (Rodríguez-Reinoso, 1998). Carbon supports are intrinsically hydrophobic and have to be made hydrophilic to increase surface wettability by polar solvents such as water and facilitate homogeneous distribution of supported metal precursors. Surface oxygen-containing functionalities act as metal-anchoring sites (Cameron et al., 1990), promote reduction of the metal precursor (Emmrich, 1999) and lower hydrophobicity and improve support accessibility during catalyst synthesis (Solís-López et al., 2014). The concentration and nature of surface groups can be tailored by treatment with oxidising agents (HNO_3, $KMnO_4$, H_2SO_4/HNO_3, $(NH_4)_2S_2O_8$, H_2O_2, and O_3) (Wepasnick et al., 2011).

Mondal et al. prepared Ag/carbon polymer hybrid films using spin coated thin films of PAN in N,N-dimethyl formamide followed by their carbonization and incorporation of a silver salt in the solution prior to spin coating. The Ag/carbon porous films were reported to be effective in the reduction of 4-NP to AP with sodium borohydride (Mondal et al., 2013). Cárdenas-Lizana et al. performed gas phase continuous hydrogenation of m-dinitrobenzene (m-DNB) over acid treated AC supported Au and Ag prepared by deposition-precipitation (Cárdenas-Lizana et al., 2015). In-situ reduction of Ag nanoparticles on oxygenated mesoporous carbon fabric was performed by Ji et al. and used for reduction of nitro aromatics (Ji et al., 2016).

Our objective was to investigate the potential of synthesised activated carbons from palm shell (SPAC, PSAC, PCAC and PAC) described in chapter 2 as supports for Agnps and investigate their potential for the catalytic reduction of Nitrophenols. 4-NP, DNP and TNP were chosen as model compounds.

3.2 Experimental

3.2.1 Chemicals and reagents

$AgNO_3$ (Spectrochem, India), $NaBH_4$ (Spectrochem, India), 4-NP, DNP and TNP (Spectrochem, India) were used. De-ionized water was used for preparation of all solutions.

3.2.2 Synthesis of NanoSilver Supported on ACs

The nano silver supported on to ACs (Agnp-ACs) were synthesised by a one pot process (Figure 3.1). The optimised protocol was: 1.25 g of AC was initially mixed with 50 mL of 0.1 N $AgNO_3$ solution for 30 min followed by addition of 0.1% (w/w of $AgNO_3$) $NaBH_4$. The whole reaction mixture was kept in dark for 4 h and then filtered through whatman filter paper no. 42, followed by washing with conductivity water until excess of $AgNO_3$ solution was removed. The residue was then allowed to dry at ambient conditions.

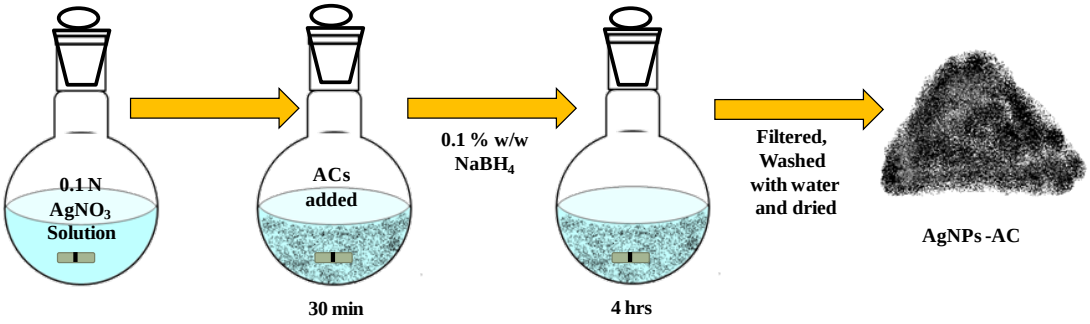

Figure3.1 Schematic presentation for the synthesis of Agnp-AC

Agnp-SPAC, Agnp-PSAC, Agnp-PCAC and Agnp-PAC were synthesized following the above protocol. The synthesis and characterisation of SPAC, PSAC, PCAC and PAC have been discussed in chapter 2.

3.2.3 Characterizations of NanoSilver Supported on ACs

All the four Agnp supported carbons were characterised by XRD, SEM-EDX, FTIR, TEM, Zeta Analyser, Raman and UV-Vis spectroscopy.

3.2.3.1 Transmission Emission Microscopic Analysis (TEM)

Aqueous solutions of Agnp-SPAC, Agnp-PSAC, Agnp-PCAC and Agnp-PAC were dried on -1500 mesh Cu coated TEM grid (Tecnai-12, FEI-Netherlands) for analysis. Images were taken by single tilt holder with CCD Camera. Tecnai software was used for noise filtering.

3.2.3.2 Raman Analysis

Raman analysis was carried out using Mini Ram-II (B&W TEK) Raman Spectrometer with "CLEANLAZE" laser technology (excitation at 785 nm) and TE cooled 2048 pixel CCD array spectrometer in the range 200 cm^{-1} to 2800 cm^{-1}. The analysis was done by taking powder samples in transparent plastic bags and liquid samples in transparent glass vials.

3.2.4 Assay of silver loaded in Agnp-ACs

About 0.1 g sample of Agnp-AC was dried in an oven at 105°C until constant weight and then digested with 10 mL nitric acid (16 M) in an evaporating dish almost to dryness; further 10 mL nitric acid was added and again digested to dryness. About 15 mL of water was added to the digest and boiled for 10-15 min; the suspension was filtered and thoroughly washed with de-ionized water. The resultant filterate and washings were combined and diluted to 10 mL with de-ionized water. The silver concentration in the obtained solution was determined using ICP-OES (Optima 3300 RL, Perkin Elmer).

3.2.5 Catalytic Reduction of Nitrophenol

The potential of Agnp-SAC, Agnp-SPAC, Agnp-PCAC and Agnp-PAC as catalysts has been evaluated for the reduction of 4-NP, DNP and TNP. Literature reports revealed that during the study of nitrophenol reduction reaction catalyzed by metal nps and semiconductor nanocomposites, the color changes involved during the reduction reaction provide simple means to monitor the reaction spectroscopically (Aditya et al., 2015; Fu et al., 2016; Ko et al., 2015; Pozun et al., 2013; Vats et al., 2016). In neutral or acidic condition, 4-NP exhibits a strong absorption peak at 317

nm. Upon addition of $NaBH_4$ to 4-NP, the increased alkalinity of the solution leads to the formation of 4-nitrophenolate ions with a new absorption band at 400 nm (Hayakawa et al., 2003; Praharaj et al., 2004).

The catalytic reduction experiment was carried out in 10 mL glass vial. In a typical setup, 0.02876 mmol 4-NP was mixed with 8 mL water followed by 20 mg of Agnps-AC and 0.7 mmol $NaBH_4$. 100 µL of reaction mixture was taken and diluted to 5 mL in a volumetric flask and the progress of reaction was monitored by taking UV-visible absorption spectra in the wave length range of 200-600 nm at regular time intervals.

3.3 Results and discussion

3.3.1 Characterization of Agnps-AC

3.3.1.1 UV-Visible spectroscopy

UV–Vis spectra of ACs or Agnp-ACs suspension was recorded on Jasco, (Japan) V-603 spectrophotometer in the wavelength range 200–800 nm against water as blank. Figure3.2 shows UV-Vis spectra of all four catalysts and their respective pristine carbons. It is observed that ACs and Agnp-ACs exhibited strong absorption in the visible light region due to their black color (Lee et al., 2015).

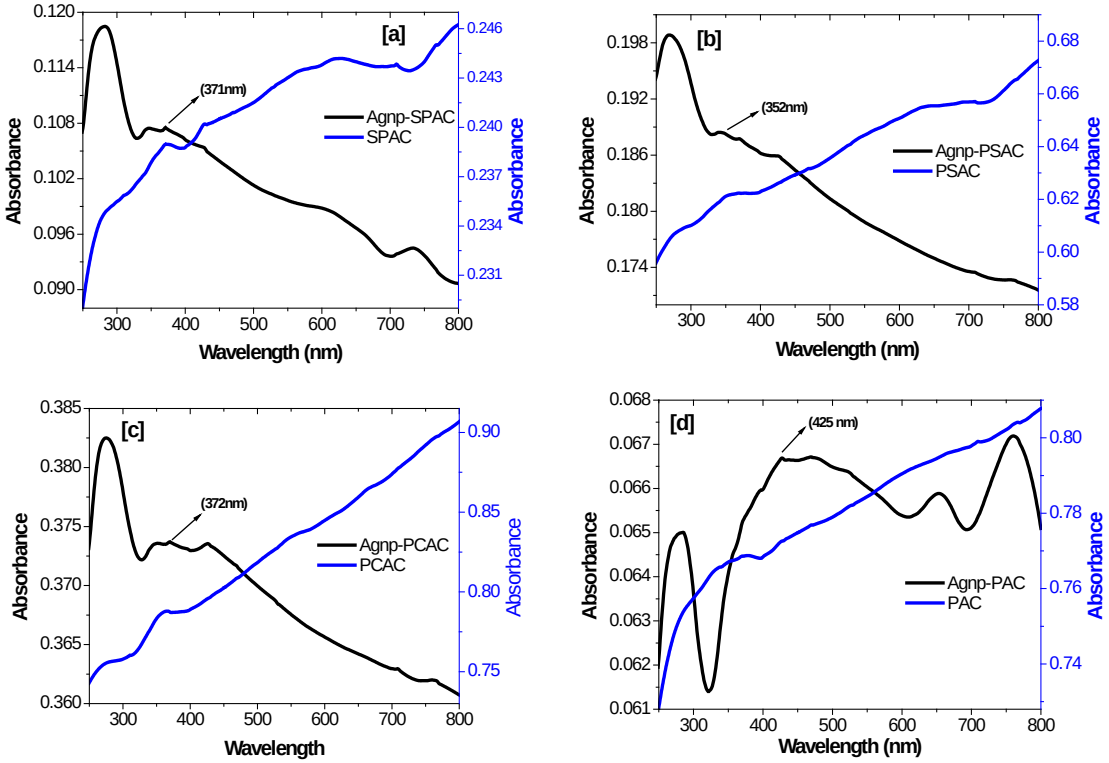

Figure 3.2 UV-Visible Spectra of ACs and Agnp-ACs

The absorption at 200-350 nm is attributed to the characteristic absorption of the AgCl while the absorption at 350-800 nm can be ascribed to the characteristic surface

plasmon resonance (SPR) absorption of Ag nps (Zheng et al., 2015). However, the weak absorbance may be due to the dispersion of Ag on the surface of ACs.

3.3.1.2 FTIR analysis

The ACs loaded with silver exhibited increase in intensity of the bands at 1102 cm^{-1}, 1180 cm^{-1} and 1402 cm^{-1} (Figure 3.3). This could be attributed to oxidation of active oxygen functionalities. Further, there was increase in intensity of the band at ~3350 cm^{-1}, representing the O–H stretching in C–OH. The band at 900–600 cm^{-1} could be assigned to Ag–O vibrations (Huang and White, 2003).

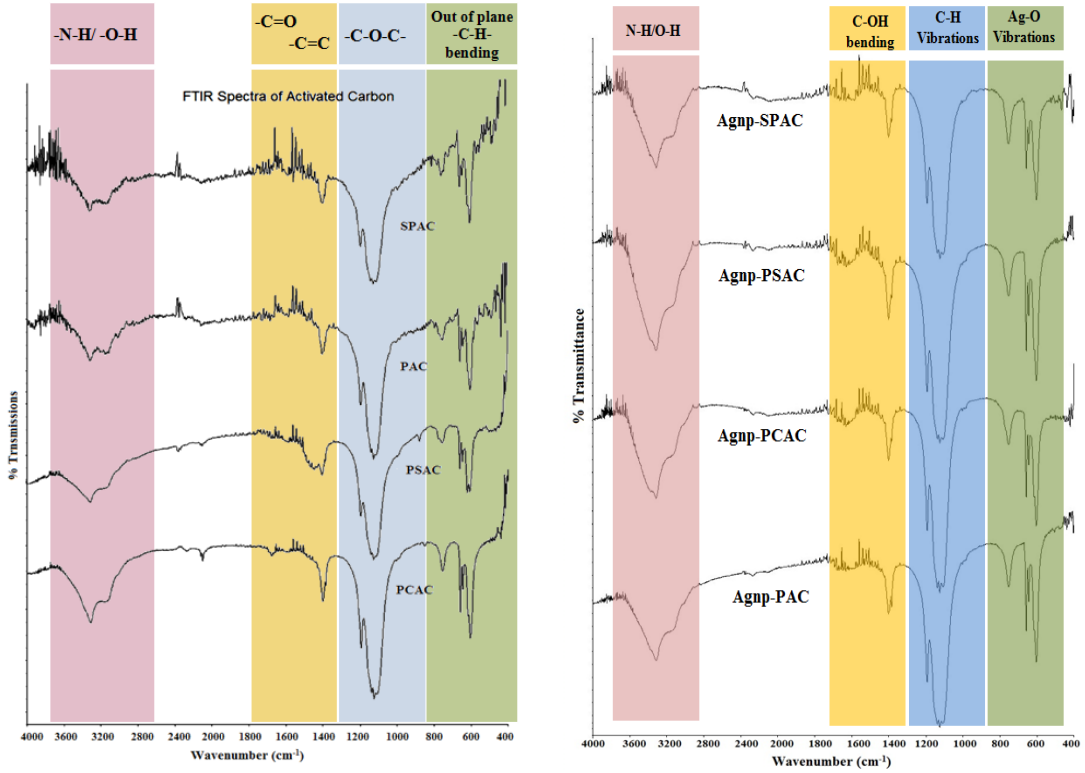

Figure 3.3 FTIR spectra of ACs and Agnp-ACs

3.3.1.3 XRD analysis

XRD patterns of as prepared catalysts are shown in Figure3.4. The well defined intense peaks in the diffraction pattern indicated crystallinity of the Agnps. Characteristic 2θ values of silver nano particles observed were 38.12°, 44.31°, 64.45° and 77.4° for Agnp-SPAC; 38.04°, 44.22°, 64.39° and 77.36° for Agnp-PSAC; 38.02°, 44.24°, 64.34° and 77.32° for Agnp-PCAC and 38.01°, 44.22°, 64.37° and 77.32° for Agnp-PAC that could be readily indexed to the (111), (200), (220) and (311) reflections of fcc structure of silver, respectively (Lu et al., 2007) while a broad diffraction peak at 2θ ~23.5° corresponds to the (002) diffraction of graphite plane arising from the carbon support. The broadness of the peak could be due to nano

crystallite size. The average crystallite size was calculated to be ~20, 52, 50, 59 nm for Agnp-SPAC, Agnp-PSAC, Agnp-PCAC and Agnp-PAC respectively. It can be seen that the crystalline silver is present in the nanometer range.

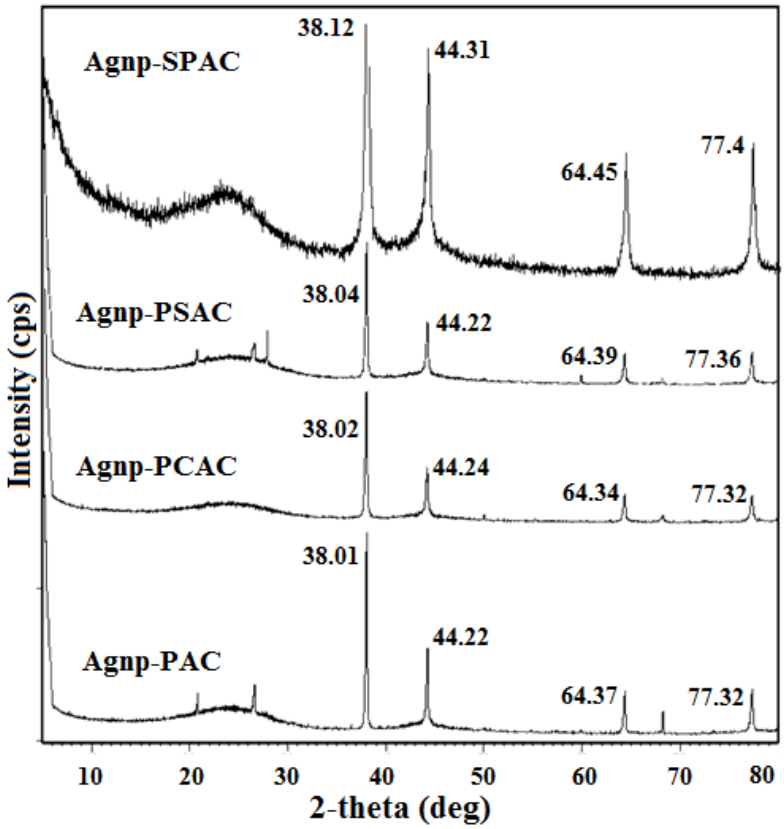

Figure 3.4 XRD spectra of Agnps-ACs

The presence of 400 plane of AgCl could be observed in AgPAC (2θ ~ 68.29°) and AgPCAC (2θ ~ 68.21°). An additional diffraction peak due to 222 plane of AgCl was observed in AgPSAC. Further, AgPAC and AgPSAC showed sharp diffraction peaks at 26.58° and 26.47° respectively due to ordered (002) plane of graphene layers overlain on the broad graphite peak. Additional peaks were observed in AgPSAC and AgPAC at 2θ = 20.76° and 20.81° respectively, probably caused by widened stacking of more wrinkled or disordered graphene layers at the edge areas (Mohammed et al., 2016).

3.3.1.4 SEM analysis

Figure 3.5 shows the SEM images of the prepared Agnps-AC. It can be seen the Agnps were deposited on the carbon surface and in the pores.

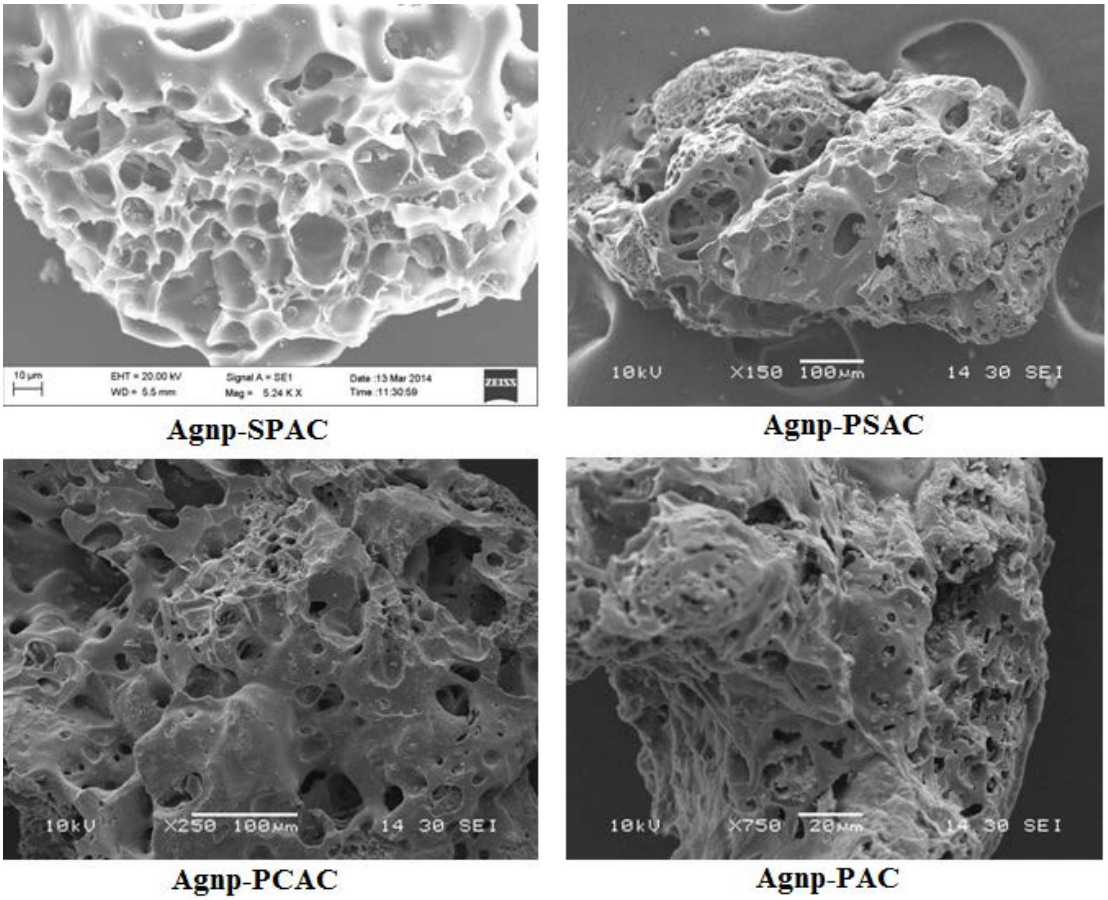

Figure 3.5 SEM images of Agnp-AC

3.3.1.5 EDAX analysis

The dispersion of Ag onto the surface of ACs was confirmed by EDAX analysis.

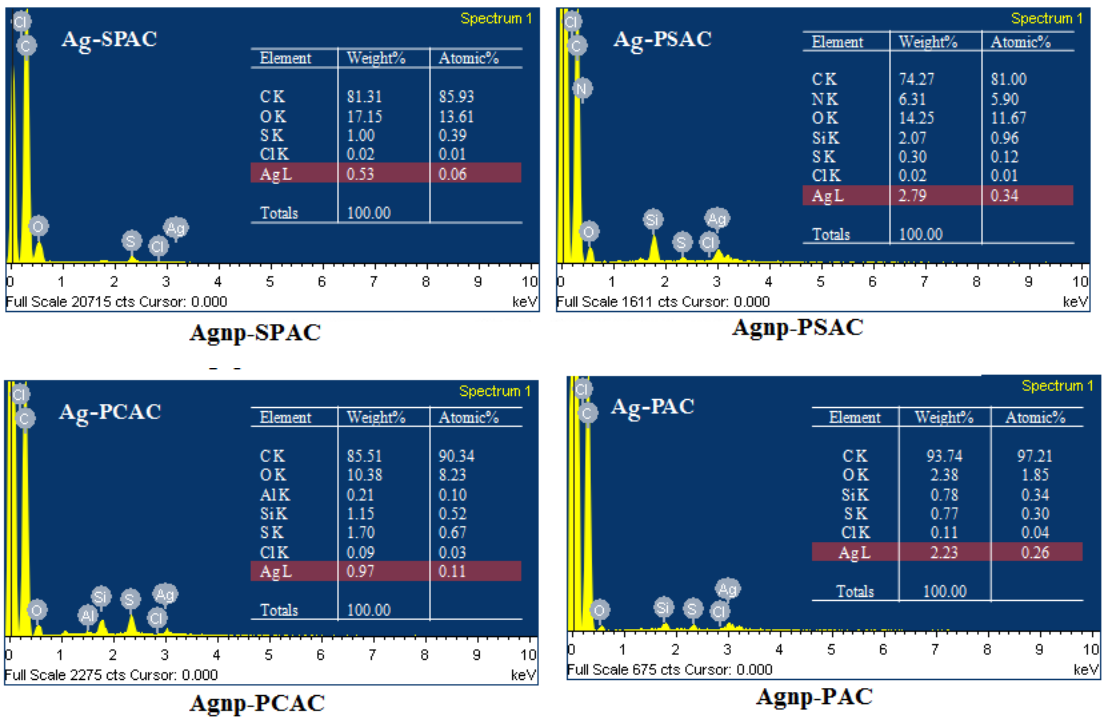

Figure 3.6 EDAX analysis of Agnp-AC

Quantitative determination of Agnps loading onto the ACs surface was also determined by ICP-OES analysis. The results are given in Table 3.1.

Table 3.1 Ag content in Agnps-ACs determined by ICP-OES

Catalyst	w/w (%) of Ag in Agnps-AC
Agnp-SPAC	4.86
Agnp-PSAC	4.23
Agnp-PCAC	1.93
Agnp-PAC	7.25

It was observed that the results were not in agreement with SEM-EDAX probably due to Ag being deposited into the pores of the carbon supports.

3.3.1.6 TEM analysis

The TEM images of all Agnp-ACs are given in Figure3.7. It can be seen that the Agnps are mainly in distorted spherical shape and the average size of Agnps in all cases was found to be less than 40nm. The multilayers of graphene are clearly visible in AgPAC amd AgPSAC suggesting that the structure of the graphene sheets appears to be retained after loading of Ag.

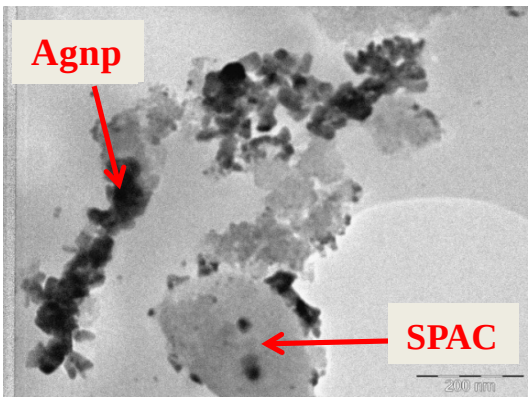

Agnp-SPAC

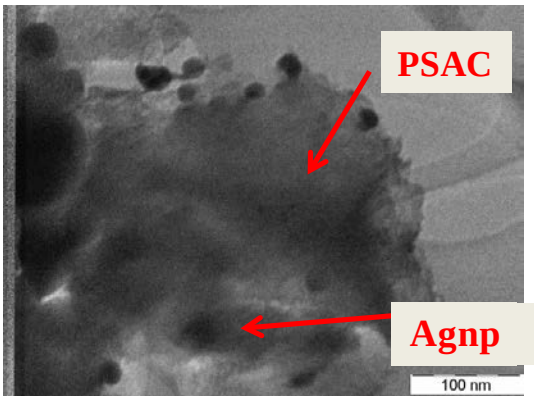

Agnp-PSAC

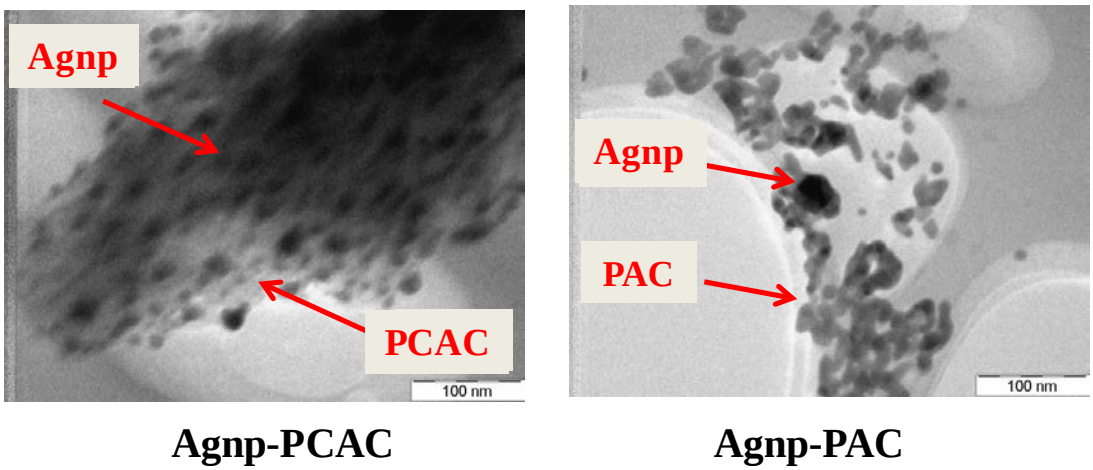

Figure 3.7 TEM images of Agnps-AC

3.3.1.7 Zeta-potential analysis

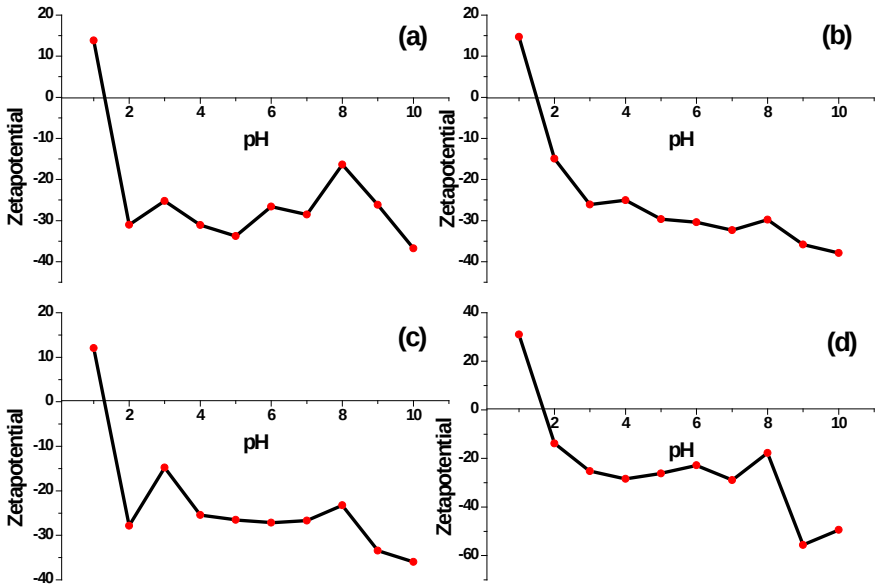

Figure 3.8 Zeta-potential analysis of Agnps-ACs; (a) Agnp-SPAC (b) Agnp- PSAC (c) Agnp-PCAC (d) Agnp-PAC

All the carbons loaded with Agnps displayed negative zeta potential from pH 2, and exhibited increasingly negative zeta potential as pH increased. It was observed that the zeta potential values of Agnps-ACs were greater than -30 mV in the pH range 9 to 10, which is an indication of the high stability of prepared Agnps-ACs against agglomeration. The high value of the zeta potential also indicates the electrostatic repulsion between the formed particles, keeping particles free from agglomeration and stable for long periods.

3.3.2 Evaluation of Catalytic Performance of Agnp-ACs for reduction of 4-NP

The catalytic activities of Agnp-ACs were investigated for the reduction of 4- NP using $NaBH_4$. About 20 mg of Agnp-AC was added to 0.02876 mmol of 4-NP solution followed by 0.7 mmol $NaBH_4$. During the reaction, the absorption peak of 4-NP underwent a red shift from 317 to 400 nm (due to the generation of 4-nitrophenolate ion) immediately upon the addition of $NaBH_4$, corresponding to a significant change in solution color from light yellow to yellow-green (Figure 3.9). The reduction process could be monitored by measurement of the absorbance at 400 nm, which is due to the formation of 4-nitrophenolate ions (Nandanwar and Chakraborty, 2012). As can be seen in Figure 3.9, with the addition of $NaBH_4$ to the mixture of 4-NP and Agnp-PCAC, the absorption band at 400 nm due to 4-nitrophenolate ion gradually decreased as the catalytic reduction reaction proceeded with simultaneous appearance of a two new absorption bands at 290 nm and 230 nm due to the formation of 4-AP.

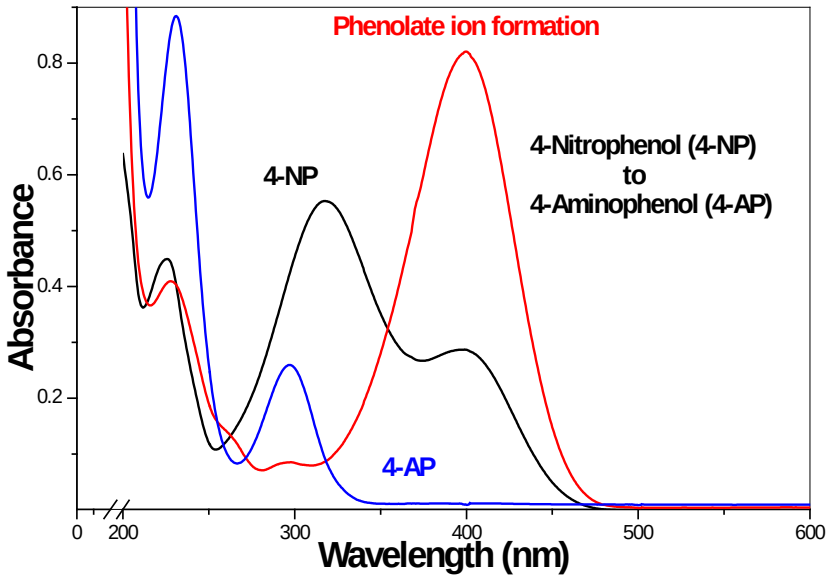

Figure3.9 Reduction of 4-NP to 4-AP via phenolate ion formation in presence of Agnp-PCAC

In the absence of Agnp-AC, peak at 400 nm remained unaltered for a long duration (Figure3.10). As can be seen from Figure3.10, complete reduction of NP to 4-AP has taken about 19 h in presence of only $NaBH_4$ indicating the extremely slow kinetics of $NaBH_4$ in reduction of 4-nitrophenolate ion.

Further, the reduction of NP was also monitored in the absence of $NaBH_4$ by taking only NP and Agnp-AC.

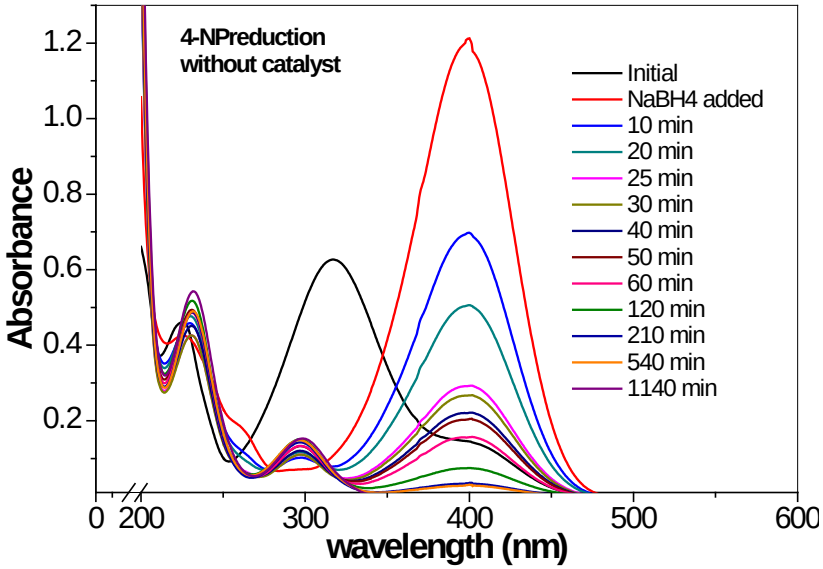

Figure 3.10 Reduction in presence of $NaBH_4$ without any catalyst

It can be seen from Figure 3.11, that that decrease in absorbance after 15 min, 7 min, 14 min and 10 min (time for catalytic reduction section 3.3.3) was 36.2%, 20.8 %, 19.8%, and 5.49 % for Agnp-SPAC, Agnp-PSAC, Agnp-PCAC and Agnp-PAC respectively which could be attributed to adsorption. However quantitative adsorption did not occur even after 24 hours.

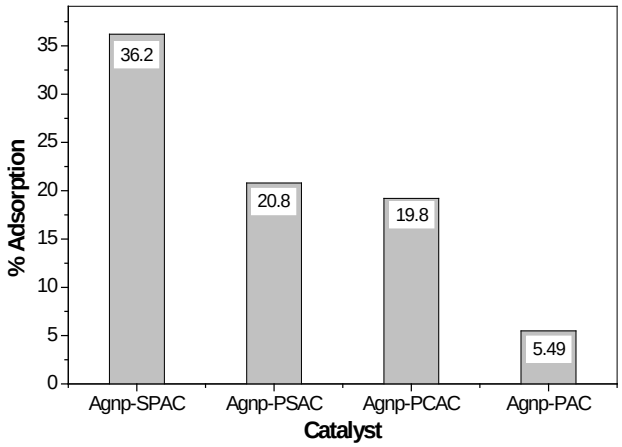

(Initial pH = 5.5, 4-NP=0.02876 mmol, Agnp-ACs =20 mg)

Figure3.11 Percentage of adsorption at the time interval required for catalytic reduction of 4 NP using only Agnp-AC under study as adsorbent

Further the effect of just pristine ACs on NP reduction taking 4-NP, $NaBH_4$ and pristine ACs (i.e. without Agnps) in the reaction mixture was investigated.

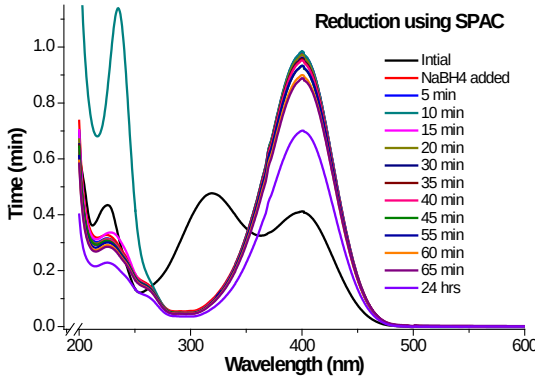

Initial pH = 5.5, 4-NP=0.02876 mmole, SPAC = 20 mg, $NaBH_4$=0.7 mmole

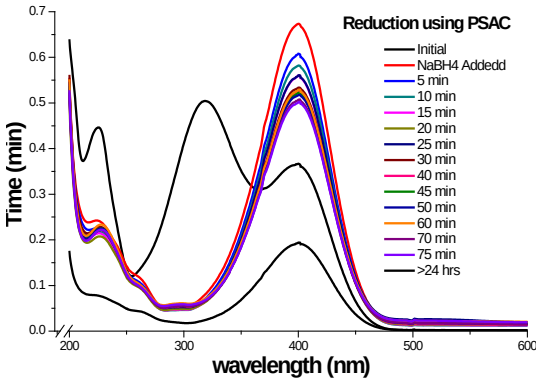

Initial pH = 5.5, 4-NP=0.02876 mmole, PSAC= 20 mg, $NaBH_4$=0.7 mmole

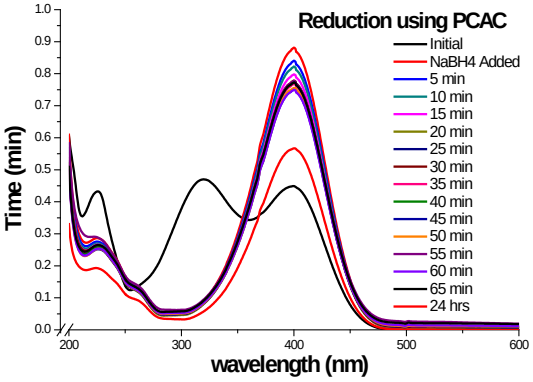

Initial pH = 5.5, 4-NP=0.02876 mmole, PCAC= 20 mg, $NaBH_4$=0.7 mmole

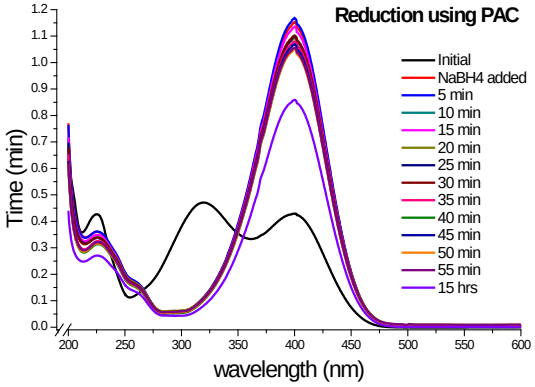

Initial pH = 5.5, 4-NP=0.02876 mmole, PAC = 20 mg, $NaBH_4$=0.7 mmole

Figure 3.12 Reduction using pristine ACs

It can be seen from Figure 3.12 that decrease in absorbance after 15 min, 7 min, 14 min and 10 min (time for catalytic reduction section 3.3.3) was 1.06%, 13.05 %, 9.45 %, and 4.46 % for SPAC, SAC, PCAC and PAC respectively. The pristine activated carbons alone were thus not functioning as catalysts and both Agnp-ACs and $NaBH_4$ were required for the effective reduction of 4-NP to 4-AP.

We further investigated the effect of the amount of four different Agnp-ACs under study and also the effect of increasing NP concentration as shown in Figures 3.13 [a] to 3.13 [b].

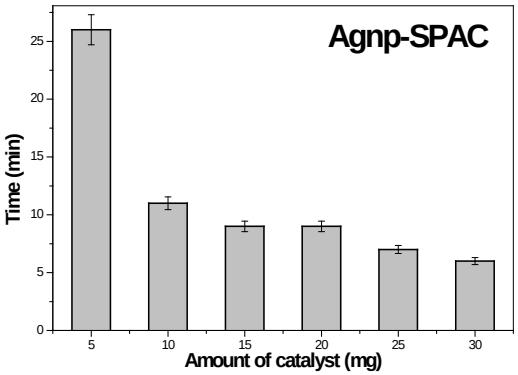

Initial pH = 5.5, 4-NP-0.02876 mmol, $NaBH_4$= 0.7 mmole, Catalyst variation 5-30 mg

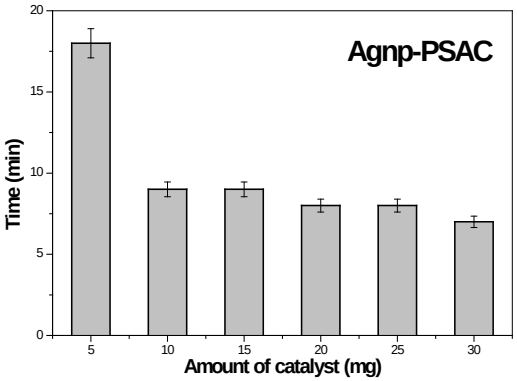

Initial pH = 5.5, 4-NP-0.02876 mmol, $NaBH_4$= 0.7 mmole, Catalyst variation 5-30 mg

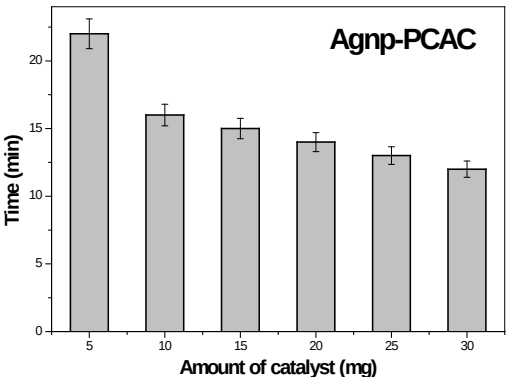

Initial pH = 5.5, 4-NP-0.02876 mmol, $NaBH_4$=, 0.7 mmole, Catalyst variation 5-30 mg

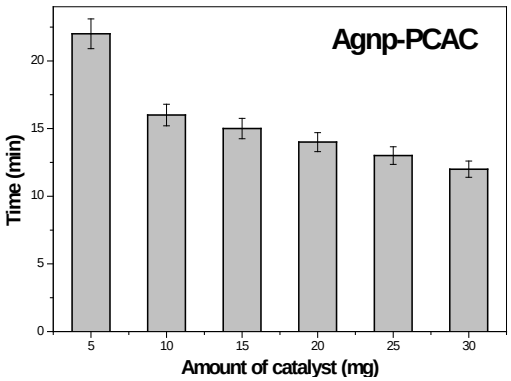

Initial pH = 5.5, 4-NP-0.02876 mmol, $NaBH_4$=, 0.7 mmole, Catalyst variation 5-30 mg

Figure3.13 [a] Effect of amount of catalyst on catalytic reduction of 4-NP

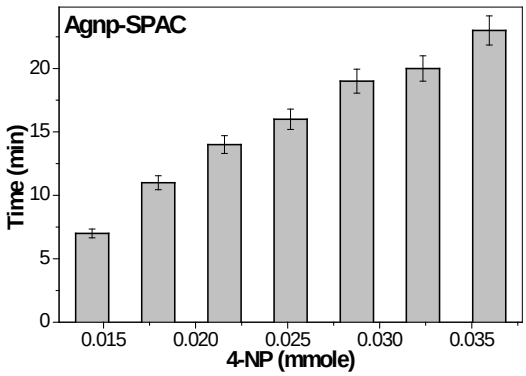

Initial pH = 5.5, Concentration of 4-NP 0.014 mmole-0.036 mmole, Agnp-SPAC-20 mg , $NaBH_4$-0.7 mmole

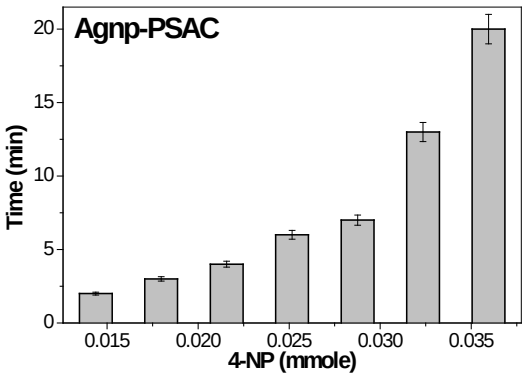

Initial pH = 5.5, Concentration of 4-NP 0.014 mmole-0.036 mmole, Agnp-PSAC-20 mg , $NaBH_4$-0.7 mmole

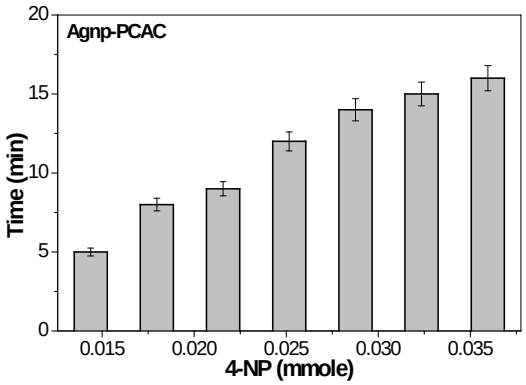

Initial pH = 5.5, Concentration of 4-NP= 0.014 mmole-0.036 mmole, Agnp-PCAC-20 mg , $NaBH_4$-0.7 mmole

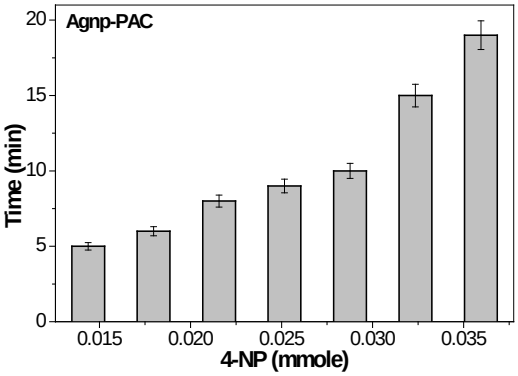

Initial pH = 5.5, Concentration of 4-NP= 0.014 mmole-0.036 mmole, Agnp-PAC-20 mg, $NaBH_4$-0.7 mmole

Figure 3.13 [b] Effect of 4-NP concentration on catalytic reduction of 4-NP

It is observed that with increasing amount of catalyst, the time taken for reduction of 4-NP was lesser. It can be further concluded from the figures that Agnp-PSAC was the most effective of all the four catalysts under study.

In addition, the product was characterised by mass spectrometry. Mass analysis also clearly suggested the presence of 4-AP with high purity (Figure3.14).

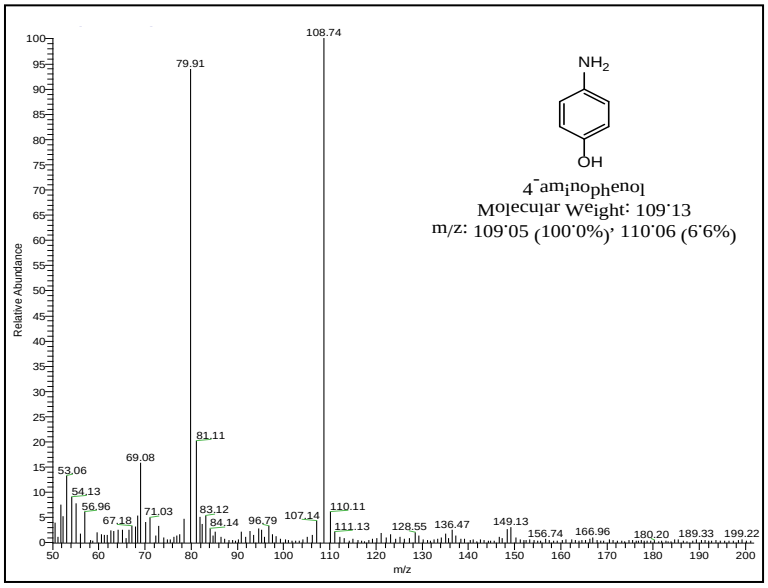

Figure 3.14 Mass spectra after catalytic reduction of 4-NP

The molecular ion which is also the base peak corresponds to m/z 109. The next most abundant ion in the spectrum is at m/z 80 attributed to pyridinium cation formed by rearrangement. The ion at m/z 53 was attributed to loss of HCN from pyridinium cation providing evidence towards the formation of aminophenol (Marín and Barbas, 2004).

Effect of sodium borohydride concentration

The reaction rate increased with increasing borohydride concentration under specific reaction conditions (Figure3.15) (Mesmer and Jolly, 1962; Wu et al., 2014).

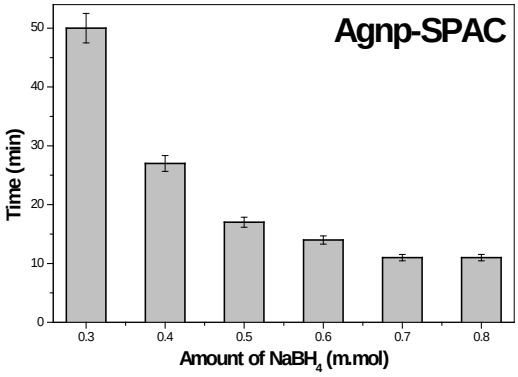

Initial pH = 5.5, 4-NP=0.01797 mmol, Agnp-SPAC=10 mg, $NaBH_4$ =0.3-0.8 mmol

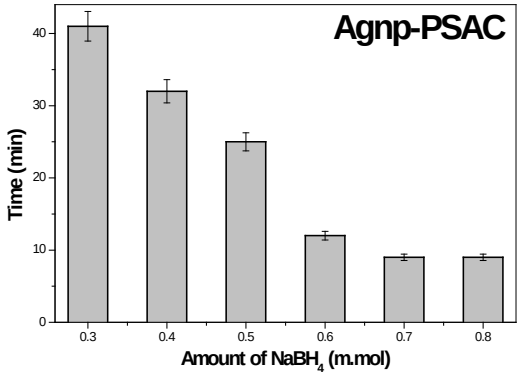

Initial pH = 5.5, 4-NP=0.01797 mmol, Agnp-PSAC=10 mg, $NaBH_4$ =0.3-0.8 mmol

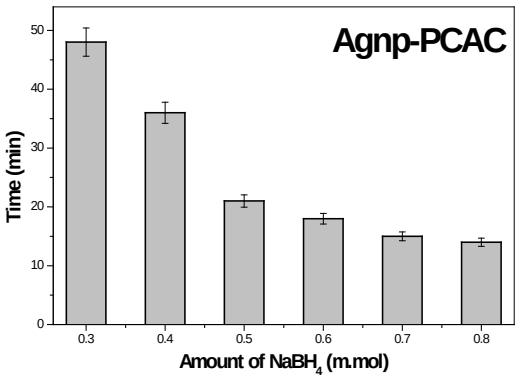

Initial pH = 5.5, 4-NP=0.01797 mmol, Agnp-PCAC =10 mg, $NaBH_4$ =0.3-0.8 mmol

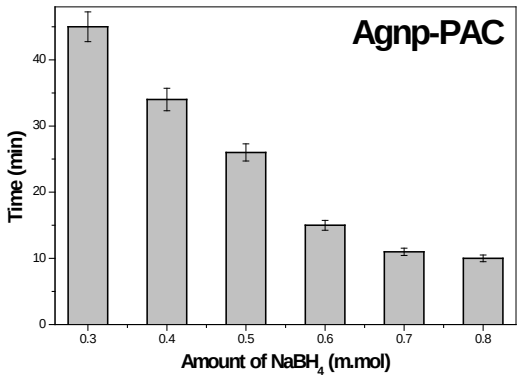

Initial pH = 5.5, 4-NP=0.01797 mmol, Agnp-PAC =10 mg, $NaBH_4$ =0.3-0.8 mmol

Figure 3.15 Effect of $NaBH_4$ variation on Catalytic reduction of 4-NP

3.3.3 Kinetic Studies of the reduction of NP by Agnp-AC

Figure3.16 displays the time-dependent UV-vis absorption spectra in the presence of all the catalysts.

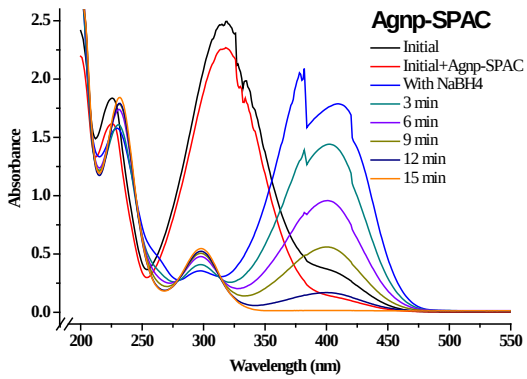

Initial pH = 5.5, 4-NP=0.02876 mmol, $NaBH_4$=0.7 mmole $_4$, Agnp-SPAC =20 mg

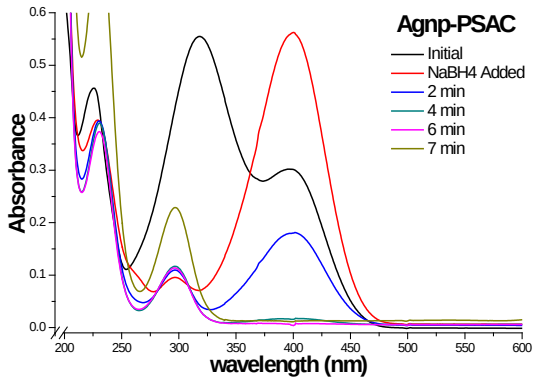

Initial pH = 5.5, 4-NP=0.02876 mmol, $NaBH_4$=0.7 mmole $_4$, Agnp-PSAC =20 mg

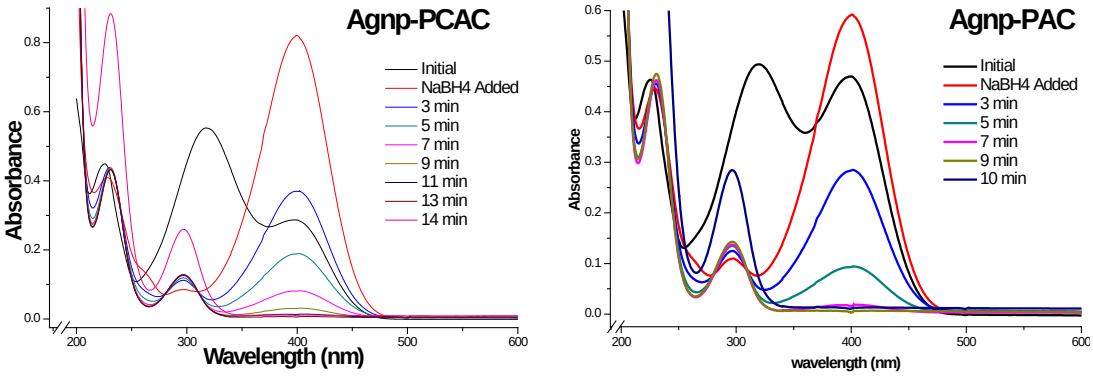

Initial pH = 5.5, 4-NP=0.02876 mmol, $NaBH_4$=0.7 mmole $_4$, Agnp-PCAC =20 mg

Initial pH = 5.5, 4-NP=0.02876 mmol, $NaBH_4$=0.7 mmole $_4$, Agnp-PAC =20 mg

Figure 3.16 Temporal evolution of UV-Vis spectra during catalytic reduction of 4-NP to 4-AP

It can be seen in all cases that, the peak of 4-nitrophenolate ions at 400 nm decreased with time along with a concomitant increase in a new peak at 299 nm indicating the formation of 4-AP (Dotzauer et al., 2009). The isosbestic points provide evidence to the formation of 4-AP as a result of reduction of 4-NP (Mei et al., 2005). At the end of the reaction, the peak for 4-nitrophenolate ion almost disappeared and only the peak for 4-AP was observed. In the present system, since the concentration of $NaBH_4$ was in excess pseudo-first-order kinetics could be applied to evaluate the kinetic rate constant (k) of the reaction (Lam et al., 2012). Figure 3.17 shows the plot of C_t/C_0 versus reaction time for the reduction of 4-NP over the catalysts; where C_t and C_0 are the concentrations of 4-NP at definite time intervals and zero time, respectively. It can be seen from Figure 3.17 that the expected linear relationship between C_t/C_0 and reaction time (t) confirmed the pseudo-first-order kinetics. The calculated rate constants and activity parameters along with literature reported values are given in Table3.1. The rate constants were observed to be comparable to literature reported catalysts for the reduction of 4- NP to 4 AP and Agnp-PSAC was found to be the most effective.

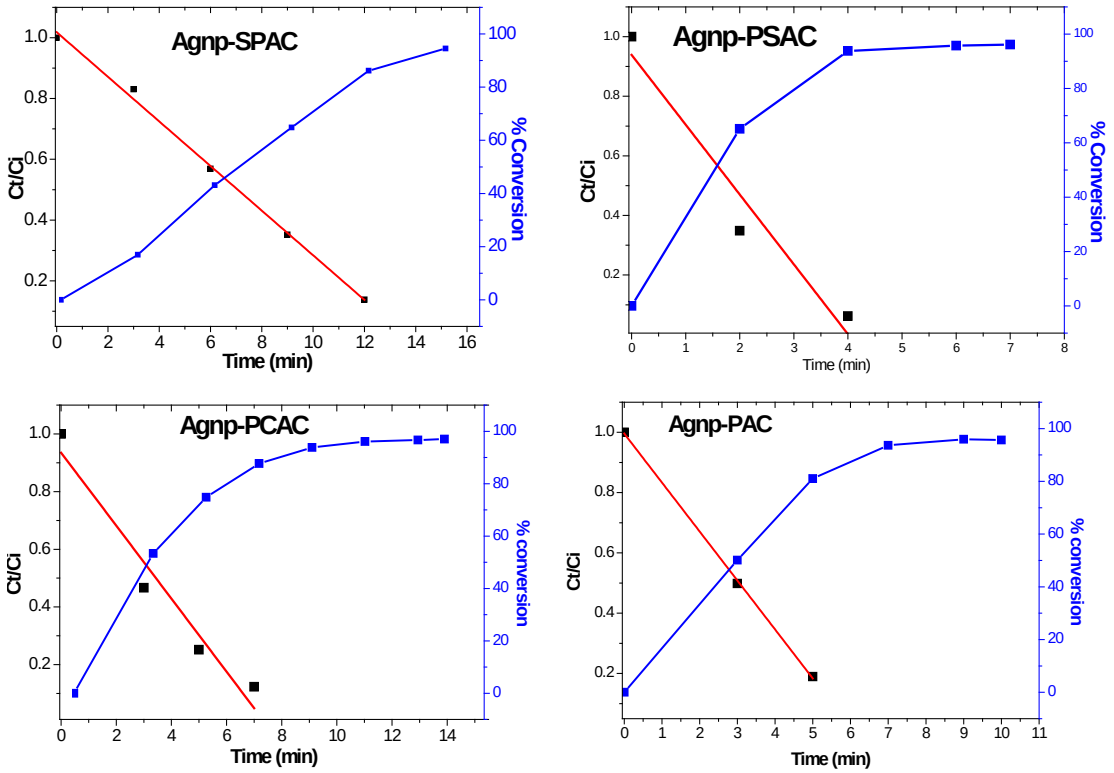

Figure 3.17 Kinetics study for the reduction of nitrophenol by Agnp-AC

Table 3.2 Results from kinetic study and their comparison with literature data

Catalyst	**weight of catalyst m (mg)**	**Rate constant k (min^{-1})**	**Activity parameter k/m (mg^{-1} min^{-1})**	**References**
Dumbbell-like Au-Fe_3O_4	2.0	0.6300	0.3150	Lin and Doong, 2011
Flower-like Au-Fe_3O_4	2.0	0.3780	0.1890	
TAC-Ag-1.0 (Silver Dendrites)	4.0	0.0218	0.0055	Rashid and Mandal, 2007
TSC-Ag-1.4 (Silver Dendrites)	4.0	0.3110	0.0778	
Agnp-SPAC	0.972	0.0734	0.0755	Present Study
Agnp-PSAC	0.846	0.2344	0.2771	
Agnp-PCAC	0.386	0.1260	0.3264	
Agnp-PAC	1.450	0.1625	0.1121	

3.3.4. Investigation of Catalyst reusability

The main advantage of this heterogeneous catalysis system was the ease of separation of the catalysts from reaction systems at the end of the reaction. Therefore, the reusability of the catalysts under study was also investigated. The reusability was tested by separating catalyst, washing it with water and after drying at 105 °C was used for the next cycle of catalysis. Figure3.18 shows the catalyst efficiency against time required for the reduction for particular cycle number. It can be seen from Figure 3.18, that for Agnp-SPAC, the time for reduction was almost constant upto 5 cycles (10 min) which increased to 12 min, 25 min and 35 min during 6th, 9th and 10th cycles respectively. When Agnp-PSAC was used as catalyst, the reduction time was 5 min. upto 4^{th} cycle which increased to 8, 15, 20 and 30 min. in 5^{th}, 8^{th}, 9^{th} and 10^{th} cycles respectively while in case of Agnp-PAC, the time required for reduction was 10 min. upto 4^{th} cycle, which increased to 20, 30 and 70 min. during 5^{th}, 6^{th} and 7^{th} cycles respectively. Agnp-PCAC was less effective in terms of its reusability as can be seen from Figure 3.18, wherein the time for reduction of 4-NP increased from 12 min. to 27 min in 3^{rd} cycle; while it took 45 min., 50 min. and 60 min. during 4^{th}, 6^{th} and7^{th} cycle respectively.

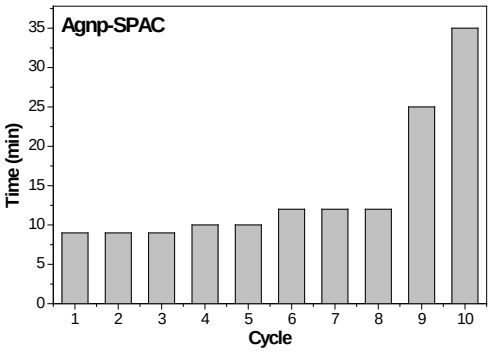

Initial pH = 5.5, 4-NP=0.02876 mmol, $NaBH_4$=0.7 mmole, Agnp-SPAC =20 mg

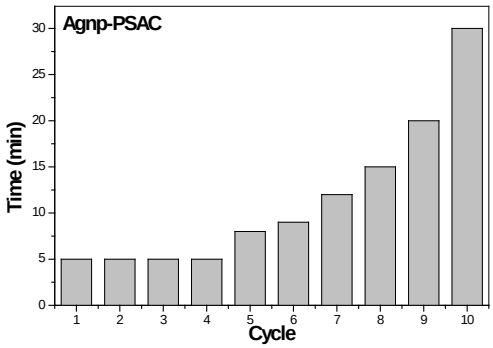

Initial pH = 5.5, 4-NP=0.02876 mmol, $NaBH_4$=0.7 mmole, Agnp-PSAC =20 mg

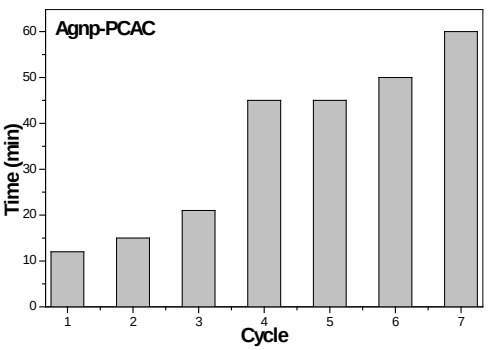

Initial pH = 5.5, 4-NP=0.02876 mmol, $NaBH_4$=0.7 mmole, Agnp-PCAC =20 mg

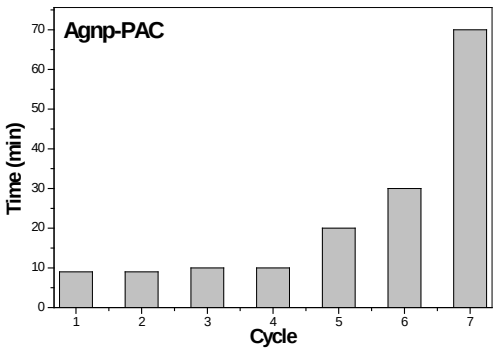

Initial pH = 5.5, 4-NP=0.02876 mmol, $NaBH_4$=0.7 mmole, Agnp-PAC =20 mg

Figure 3.18 Catalysts Reusability study

The morphology of the catalysts after each cycle and the silver content was examined by SEM-EDAX. As evident from figure 3.19 (a-d), after 4 runs, the Ag content was reduced by ~ 0.14 weight % (from 1.52 to 1.28 weight %) in case of SPAC; ~ 0.06 weight % (from 0.46 to 0.40 weight %) in case of PSAC; 0.41 weight % (from 3.84 to 3.43 weight %) in case of PCAC and 0.68 weight % (from 4.97 to 4.29 weight %) in case of PAC. The results suggest that (i) the catalysts SPAC and PSAC are more stable; (ii) there is negligible leaching of Ag from the catalysts. Hence, the catalysts under study are stable and reusable for the reduction of nitrophenols.

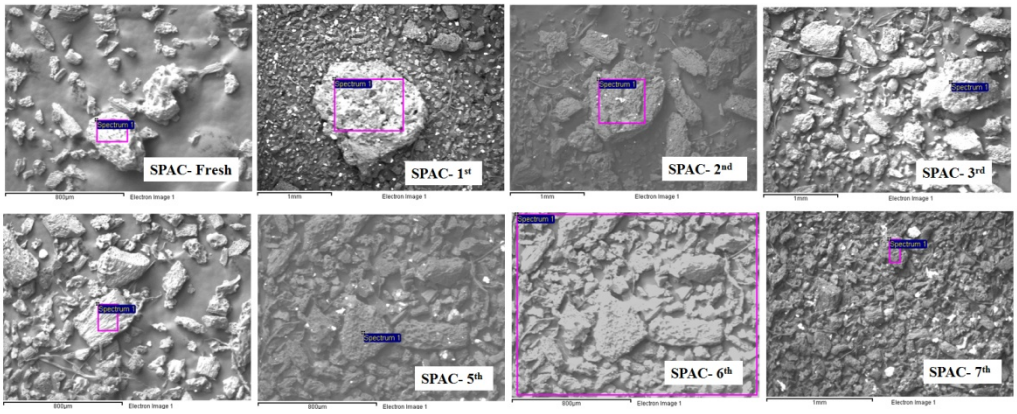

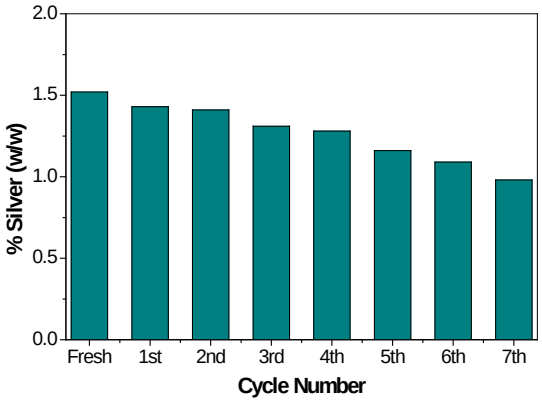

Figure 3.19 (a) SEM-EDAX analysis of Agnp-SPAC for reusability

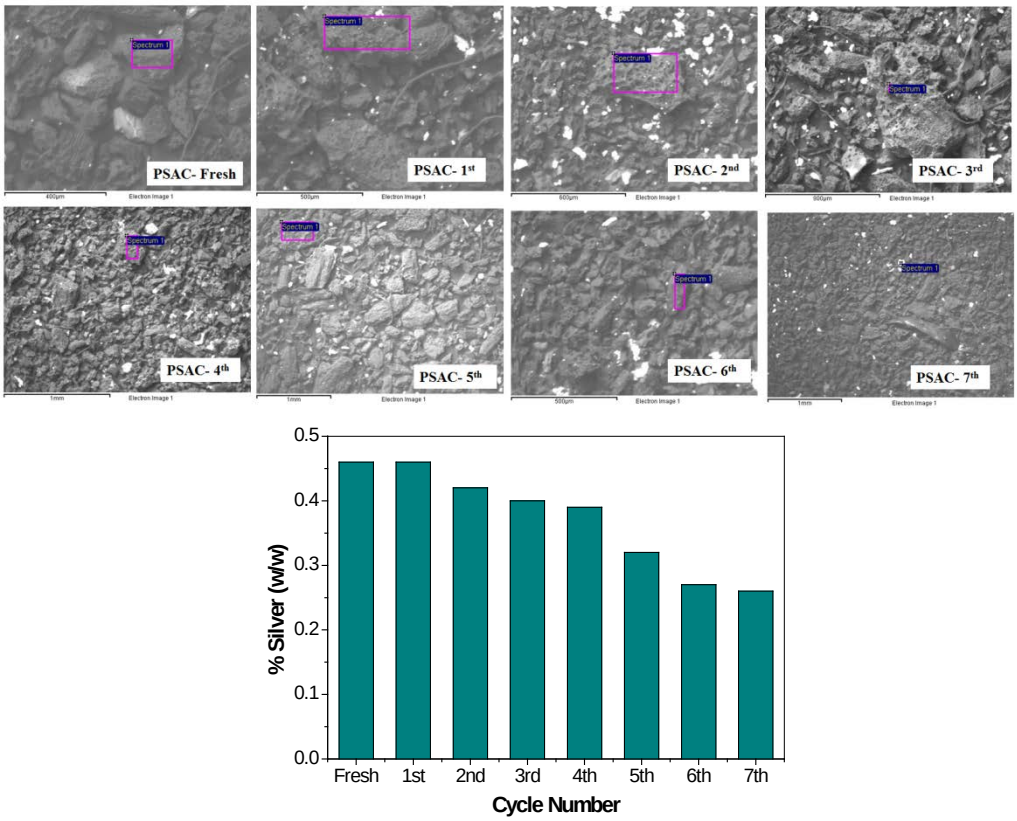

Figure 3.19 (b) SEM-EDAX analysis of Agnp-PSAC for reusability

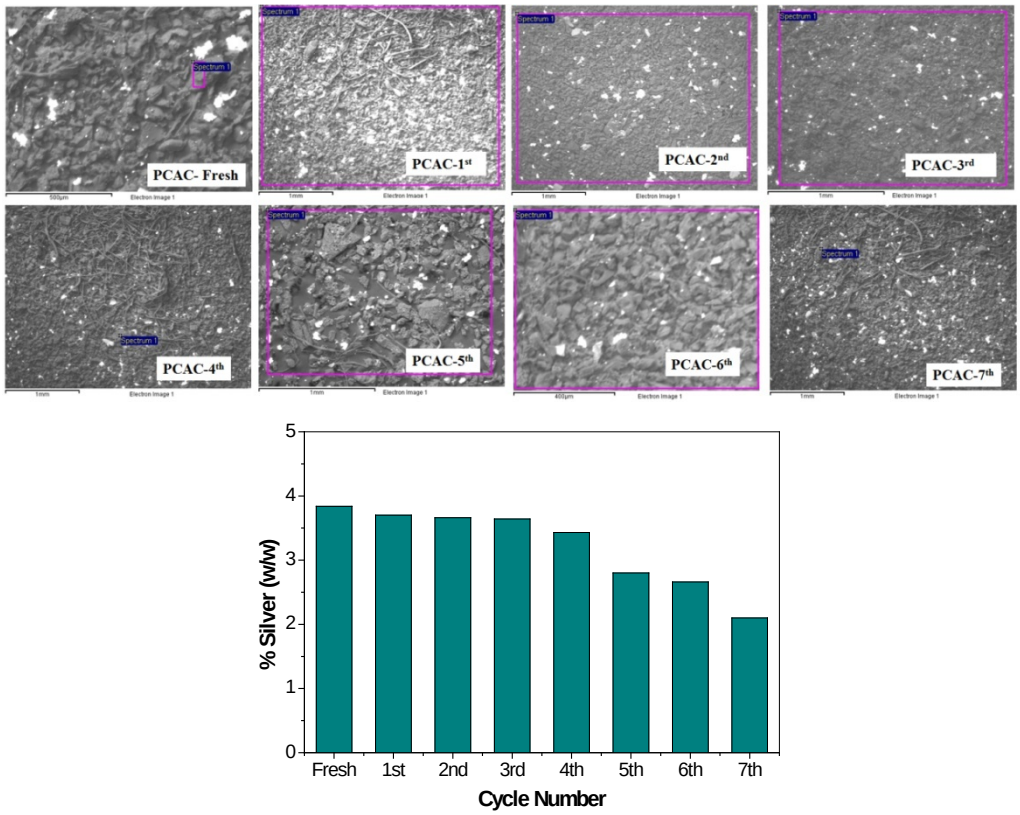

Figure 3.19 (c) SEM-EDAX analysis of Agnp-PCAC for reusability

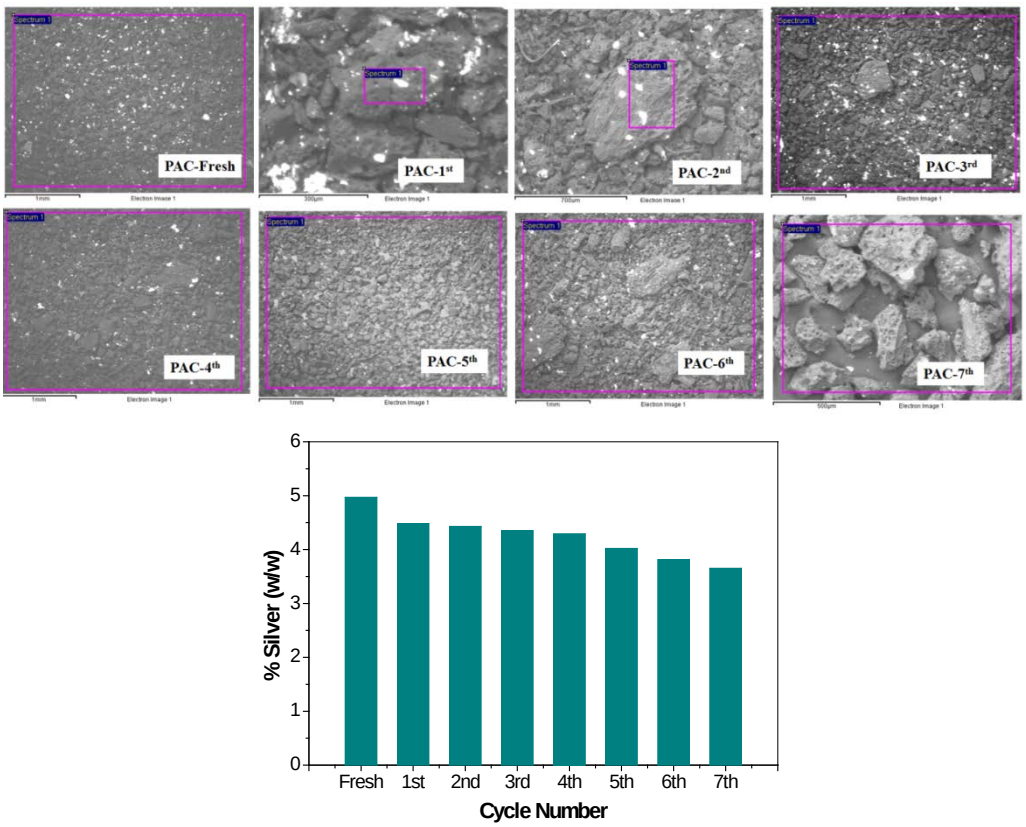

Figure 3.19 (d) SEM-EDAX analysis of Agnp-PAC for reusability

3.3.5. Raman spectral study

The Raman spectra of pristine ACs, Agnp-ACs and NP loaded Agnp-ACs are shown in Figure3.20. The samples exhibited two graphite related bands, which corresponded to the well known D (~1339$\pm$ 20 cm^{-1}) and G (~1529 $\pm$ 20 cm^{-1}) bands, assigned to defects and edge effects in sp^2 hybridized carbon lattices and to the C-C bond stretching, respectively. Significant displacement of D and G bands between the ACs and Agnp-ACs samples was not observed. The G band was assigned to the amorphous graphitic phase which is attributed to the interstitial defects (Ferrari et al., 2006). The 2D band, a D band overtone, is related to the crystallinity of the material. The intensity ratio R of the D- and G-bands (I_d/I_g) indicates a relative disorder in the carbonaceous structures (Fonsaca et al., 2015; Mehl et al., 2015). It should be noted that an Id/Ig value > 1 indicated the transition from graphite to nanocrystalline graphite (Ferrari and Robertson, 2000). The Id/Ig ratio indicated amorphous character. The down shifting of G peak position was attributed to the bond angle disorder in the graphite (Jawhari et al., 1995).

It was observed that intensity of Raman signals PSAC, SPAC, PCAC and PAC increased when loaded with Agnps. Similarly, Mehl and coworkers reported that

Raman signals of rGO or GO were increased by attached noble metallic NPs, carbon nanotubes attached to metallic nanostructures also displayed enhancement(Mehl et al., 2015). As shown in Figure 3.20, the R values increased with Ag loading for PCAC and PAC and decreased with Ag loading in SPAC and PSAC, suggesting interaction between the Ag and ACs. The R value was highest in Agnp-PCAC, where there were more Agnps loaded as seen from ICP analysis.

A few less intense bands, namely 2D (~2630 cm^{-1}) and D + D_0 (~2730 cm^{-1}), were also observed in SPAC and PAC (Figure 3.20) and were similar to those previously observed by Mehl (Mehl et al., 2015) in graphene Ag nanoparticles. The 2D band, a D band overtone, is related to the crystallinity of the carbon material (Fonsaca et al., 2015; Mehl et al., 2015).

On the right side of Raman spectra, all samples exhibit low intensity signals in the range of 2200–3500 cm^{-1} (Figure3.20), namely 2D (~2630 cm^{-1}) and D + D_0 (~2733 cm^{-1}). According to Cuesta et al, (Cuesta et al., 1994), this range is attributed to second-order spectra, i.e. overtone and combination of graphitic lattice vibration modes.

Thus, the increased intensity of AC bands in the presence of Agnps may indicate that PSAC and PAC can be used as substrates for SERS (Fonsaca et al., 2015; Mehl et al., 2015).

The occurrence of bands with medium intensity at 1339 and 1260 cm^{-1}, could be attributed to the presence of neutral nitrophenol molecules. The downshift of the nitro group stretching mode from 1359 cm^{-1} in the 4-NP loaded Agnp-ACs suggest that the adsorption onto Ag NPAC could occur via nitro group. The assignments of peaks due to 4-NP are given in Table3.3 and the Raman spectral analysis of Agnp-ACs are summarized in Table 3.4.

Table 3.3 Raman spectral analysis of 4-NP

Raman shift	Assignment
642	C-C-C out-of-plane bending
879	Ring breathing
1129	C -NO_2 stretch
1359	Sym. stretch NO_2
1522	Asym. stretch NO_2
1615	C-C stretch

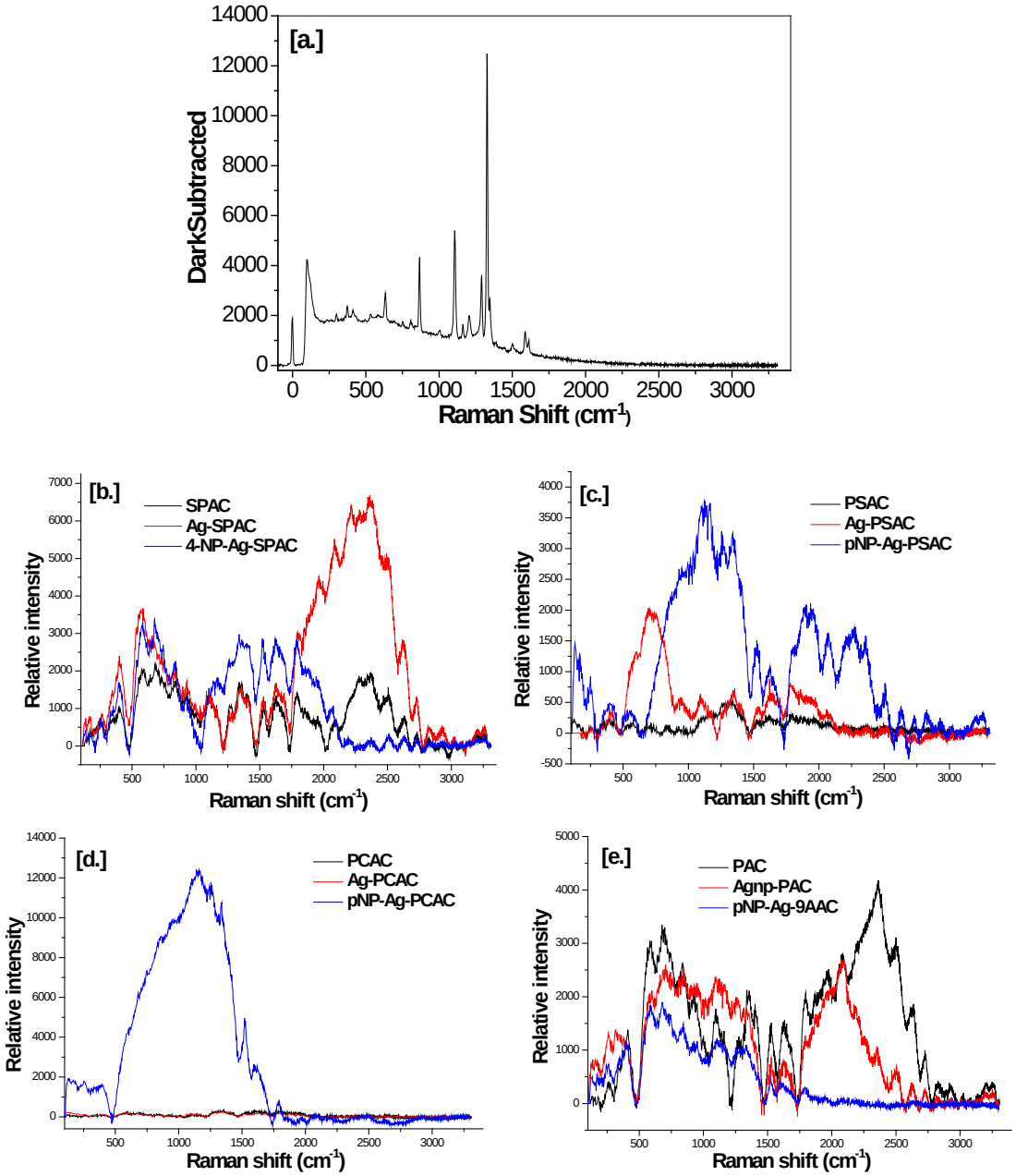

Figure 3.20 Raman spectral study of ACs, AgACs and 4-NP Loaded Ag-ACs (a) 4-NP, (b) Agnp-SPAC, (c) Agnp-PSAC (d) Agnp-PCAC (e) Agnp-PAC

Table 3.4 Raman spectral analysis of Agnp-ACs

Raman Shifts								Inference
SPAC	**AgnpsPAC**	**PSAC**	**AgnpPSAC**	**PCAC**	**AgnpPCAC**	**PAC**	**AgnpPAC**	
1104.64	1364.49	1193.94	1101.89	1101.89	1121.08	1104.64	1101.89	The D_4 band is as a result of lattice vibrations corresponding to sp^2 - sp^3 bond
1339	1364	1341	1354	1354	1334	1384	1336	Fundamental D band activated by the defects that creates holes in the π valence band (Couzi et al., 2016)
1529.59	1543.67	1527.24	1546.01	1543.67	1517.8	1529.59	1529.59	D_3 band attributed to amorphous carbon
1628.77	1642.30	1619.71	1621.98	1608.34	1633.29	1649.04	1649.04	Broad G band-in-plane vibration stretching of the C-C bond in graphitic materials and is common to all sp^2 carbon materials along with D_2 due to im plane defects
2506.38	2512.17	-	-	-	2499.1	2500.56	2504.92	Second harmonic of D_4 band
2632 weak	2643 intense	-	-	-	-	2636 moderate	2434 weak	2D band
2731.81	2733.04	-	-	-	-	2733.04	2735.51	2D overtone
I_d/I_g ratio								
1.58	1.22	2.47	1.83	1.47	1.79	1.34	2.05	

The spectra consist of peaks in the first and 2nd order regions. All peaks are narrow but superimposed on a "halo" as observed by Voranov and Street (Voronov and Jr., 2010). The G band is broad due to disorder. In-plane defects (Jorio et al., 2009; Lucchese et al., 2010) and small cluster size (Cançado et al., 2007) are both known to broaden the G band.

Combination bands in the range of 1650 -1800 cm^{-1} of high intensity were observed in SPAC and PAC and were of weak intensity in PSAC and PCAC These weak bands have been assigned to the out-of-plane combination (LO + ZA, LO + ZO') and overtone (2ZO) phonons (Araujo et al., 2012; Cong et al., 2011; Rao et al., 2011; Sato et al., 2011). The most intense band at 1750 cm^{-1}, belongs to the LO + ZO' combination mode.

The second order Raman spectra are observed only in SPAC and PAC situated at ~2500 cm-1 (D + D'') and ~2730 cm^{-1} (2D). The 2D is the harmonics of Raman inactive fundamental modes in ordered carbons (Couzi et al., 2016) the 2D band is asymmetric and comprises at least two bands due to 3D graphitic ordering (AB stacking) of the crystallites (Larouche and Stansfield, 2010) one below 2700 cm^{-1} and another above 2700 cm^{-1}; They show a peak intensity ratio of roughly one half. For very disordered carbons, the second-order bands tend to disappear (PSAC and PCAC). SPAC and PAC have high graphitization degree.

In PAC, it was possible to find peaks at 699 and 840 cm^{-1} in the ZO mode range. The in-plane modes, especially the LO + TA mode with a maximum at 1975 cm^{-1} , was of significant intensity. It is possible to find only some weak structure for the ZO' mode in a frequency range of 90 to130 cm^{-1} attributed to the breathing between layers of multilayer graphene (MLG). These peaks were less prominent in SPAC and PSAC suggesting that some MLG crystallites are interspersed in carbon matrix while in PCAC the peaks were not observed (Niilisk et al., 2016).

3.3.6. Reduction of DNP and TNP

The effectiveness of the catalysts was also investigated for reduction of DNP and TNP using the optimised conditions for NP using all the four catalysts under study. It was observed that with increase in number of nitro groups the amount of $NaBH_4$ required was higher (1.8 mmol and 2.3 mmol for DNP and TNP respectively).

The time dependent UV-Visible spectra for DNP and TNP are given in Figure3.21 (a-d).

It can be seen from the Figure 3.21 (a-d), that all four catalysts under study showed their potential for reduction of DNP and TNP. The catalytic reaction was monitored by UV-Visible spectroscopy and it was found that like 4-NP, red-shift was observed with the addition of $NaBH_4$ due to formation of the respective phenolate ions of DNP and TNP. The peak at 360 nm and 357 nm had shifted to 440 nm and 390 nm in case of DNP and TNP respectively, which gradually decreased with increase in time and new peaks developed at 300 nm and 298 nm respectively due to formation of respective amino compounds.

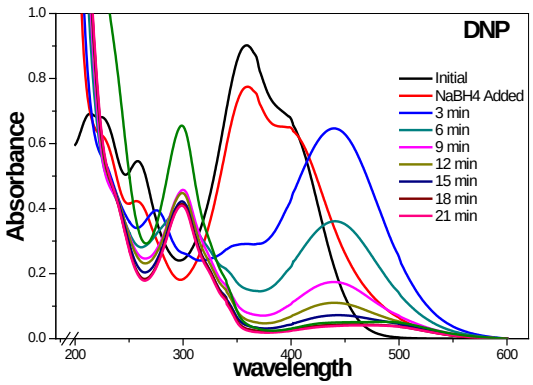

Initial pH = 5.5, DNP= 0.02876 mmol, $NaBH_4$=1.8 mmole, Agnp-SPAC= 20 mg

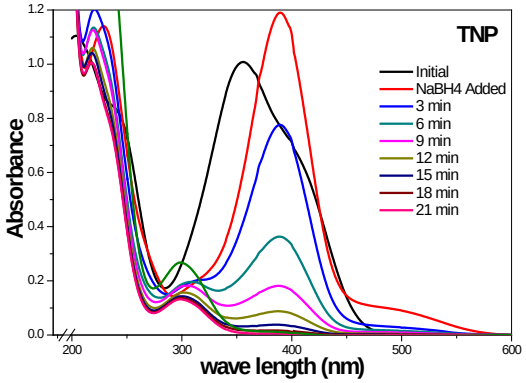

Initial pH = 5.5, TNP= 0.02876 mmol, $NaBH_4$=2.3 mmole, Agnp-SPAC = 20 mg

Figure3.21 (a) Catalytic reduction of DNP and TNP using Agnp-SPAC

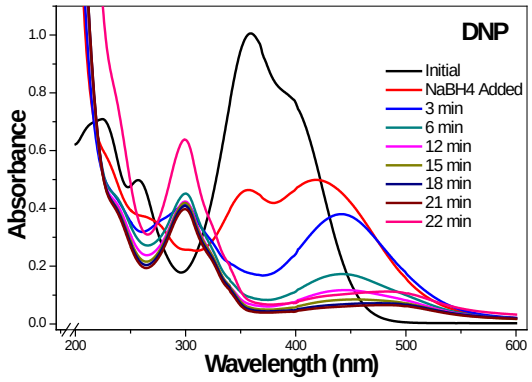

Initial pH = 5.5, DNP=0.02876 mmol, $NaBH_4$=1.8 mmole, Agnp-PSAC= 20 mg

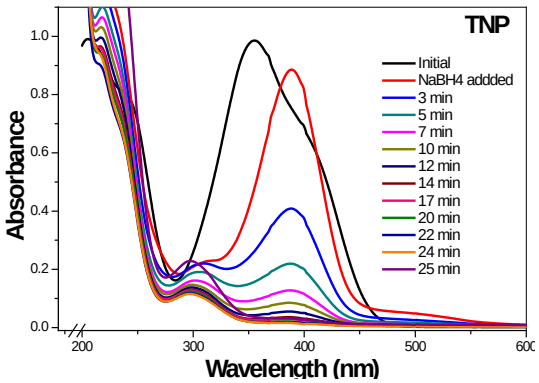

Initial pH = 5.5, TNP= 0.02876 mmol, $NaBH_4$=2.3 mmole, Agnp-PSAC= 20 mg

Figure3.21 (b) Catalytic reduction of DNP and TNP using Agnp-PSAC

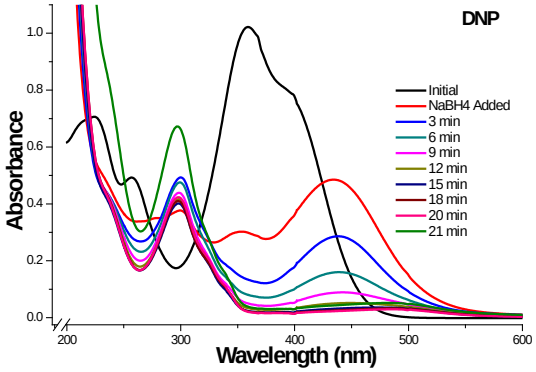

Initial pH = 5.5, DNP=0.02876 mmol, $NaBH_4$=1.8 mmole, Agnp-PCAC= 20 mg

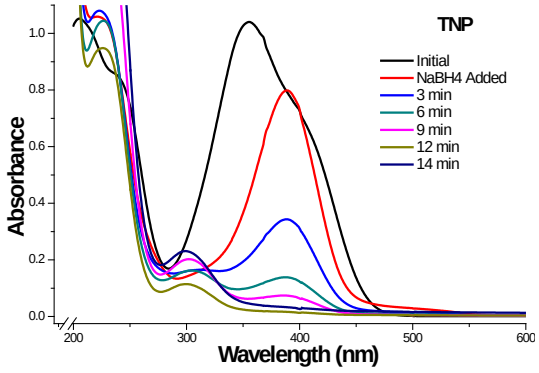

Initial pH = 5.5, TNP= 0.02876 mmol, $NaBH_4$=2.3 mmole, Agnp-PCAC= 20 mg

Figure3.21 (c) Catalytic reduction of DNP and TNP using Agnp-PCAC

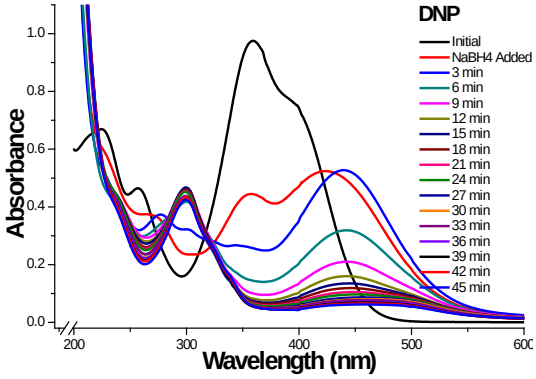

Initial pH = 5.5, DNP=0.02876 mmol, $NaBH_4$=1.8 mmole, Agnp-PAC= 20 mg

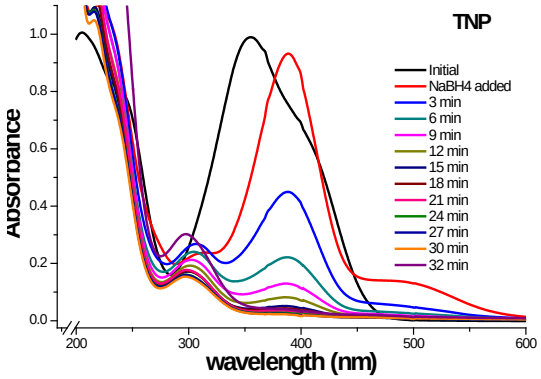

Initial pH = 5.5, TNP= 0.02876 mmol, $NaBH_4$=2.3 mmole, Agnp-PAC= 20 mg

Figure3.21 (d) Catalytic reduction of DNP and TNP using Agnp-PAC

On complete reduction no peaks were observed at both 440 and 390 nm for DNP and TNP which suggest complete reduction of respective nitrophenols.

3.4 Proposed Mechanism of Reduction of 4-Nitrophenol to 4-Aminophenol by $NaBH_4$ and rationale for the protocol adopted

Though the reduction of 4-NP by borohydride has been frequently used to examine the catalytic activity of metal nanoparticles, the mechanism of these reactions is not very clear yet. There could be several possible pathways for reduction of nitrophenol by $NaBH_4$ in the presence of metal catalyst and different researchers have proposed different mechanisms.

The reactions are usually accompanied by a time lag in observing any visible absorbance change, i.e., induction time (Saha et al., 2010; Santos et al., 2012). Various models have been reported to explain the delay, such as the time required for

borohydride molecules to diffuse to the nanoparticle surface, for the removal of surface oxidized layers (Pradhan et al., 2002), for the scavenging of the dissolved oxygen (Saha et al., 2010), for the decomposition of borohydride on the surface of nanoparticles (Khalavka et al., 2009), or the reconstruction of nanoparticles (Wunder et al., 2010).

One possible mechanism was explained by Langmuir-Hinshelwood model where in the BH_4^- ions transfer the surface-hydrogen species to the Agnps and the concomitant adsorption of 4-NP on the surface of Agnps led to the reduction of 4-NP by the surface-hydrogen species (Edison and Sethuraman, 2013). The catalysis mechanism was also attributed to the electron transfer from the donor BH_4^- ion to the acceptor nitro compounds through silver nanoparticles as mediators (Huang et al., 2012).

Choi et al. reported that charge played an important role in the activation of sodium borohydride on the surface of metal nanoparticles. Negatively charged nanoparticles prevented the approach of borohydride anions, leading to the widely reported induction time. However, they also observed that aged borohydride showed no induction time when reducing 4-nitrophenol in the presence of metal nanoparticles (Choi et al., 2016).

In contrast we observe that though Agnp-ACs under study were negatively charged there was no induction time and we could see decrease in absorbance (17.2%, 67.8%, 54.9% and 51.9% for Agnp-SPAC, Agnp-PSAC, Agnp-PCAC and Agnp-PAC respectively) immediately. We had also observed that adsorption process did not play a significant role in the time interval required for catalytic reduction of Nitrophenol (15min, 7 min, 14 min and 10 min for Agnp-SPAC, Agnp-PSAC, Agnp-PCAC and Agnp-PAC respectively).

Choi et al. had also observed that during catalysis with silver ions to catalyze the reduction of 4-nitrophenol by borohydride, the induction time shortened and the reaction constant increased with aging time of borohydride However, when they used "old" borohydride, the induction time disappeared in their experiments. Choi et al. suggested that the intermediates $B(OH)_4^-$ and $(BH_3OH)^-$ formed from the hydrolysis of borohydride were the key components that reacted with silver species during the catalysis (Choi et al., 2016).

We had added solid sodium borohydride to a solution containing 4-NP and catalyst so that hydrogen generated is used efficiently for hydrogenation of nitrophenol as soon as sodium borohydride is in contact with water resulting in complete reduction of 4-

NP in 8 to 12 minutes. The immediate utilization of hydrogen would further enhance the production of hydrogen shifting the equilibrium to the right. Recently a number of reports concerning the solid state hydrolysis of $NaBH_4$ has been published (Mäkinen et al., 2012; Mohring et al., 2009; Shurtless et al., 2009; Zhu et al., 2007). The intermediates reported by Choi et al. could be playing a role in our case as well but with no induction time as the generation of the neutral intermediate of borohydride is strongly pH-dependent and amount of water. The lower the pH, faster the hydrolysis of borohydride.

During the experiment, we found that when solid $NaBH_4$ was added to a solution containing 4-NP and Agnp-ACs a large amount of hydrogen liberation was observed on the surface of Agnp-ACs instantaneously, which came from the decomposition of $NaBH_4$ indicating that Agnps catalyze the decomposition reaction.

The pH of the medium is initially ~ 5 where the NP existed mainly in molecular form whose pKa value is 7.15, and the adsorption of 4-NP was ascribed to the hydrophobic interaction, hydrogen bond between the nitro, hydroxyl groups in 4-NP molecules and hydroxyl, carboxyl groups on adsorbent surface, and dispersion interaction between the aromatic ring and the basal planes of AgAC (section 2.6 in chapter 2). However, the amount adsorbed is less in the short time interval. On the other hand, the yielded H_2 molecule due to direct interaction of AgAc with $NaBH_4$ powder is bound to the surface of Agnps and its antibonding molecular orbital accepts the electron pairs donated by d electrons of Ag atom. Thus the bond order of H_2 declines which results in activation of the H_2 while nitro group coordinates with nano Ag and donates the electrons from oxygen to the unoccupied orbitals of Ag. The reduction proceeds when nitro aromatics and activated H_2 are absorbed chemically on the surface of Ag NPs. In this case, Ag NPs served as mediators of electron transfer(Figure 3.22). The immediate reduction of NP and desorption from surface further promotes more nitrophenol to be adsorbed and further reduction to take place. With increase in time the hydrolysis products of borohydride would also be playing a role in the reduction of NP as observed by Choi et al. (Choi et al., 2016).

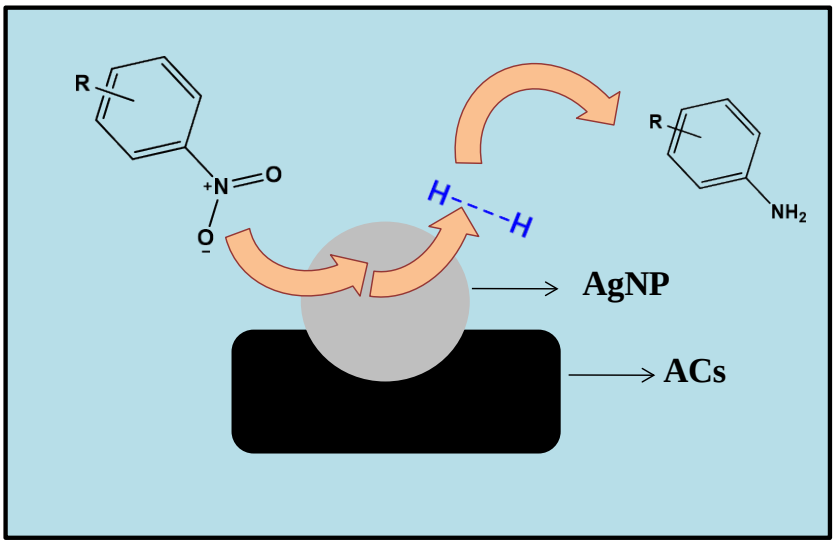

Figure3.22 Proposed Mechanism for the Nitophenol reduction

3.5 Conclusions

Silver nanoparticles were loaded onto SPAC, PSAC, PCAC and PAC by a one pot synthesis using $NaBH_4$. Transmission electron microscopic images show that Ag nanoparticles with the mean particle size of around 20-40 nm were well-dispersed on the Agnp-ACs while the XRD analysis of Agnp-ACs revealed loading of Agnps by giving sharp crystalline peaks at 38.2˚ and 44.1˚. The as-prepared Agnp-ACs were used as effective catalysts for the reduction of nitrophenols to aminophenols from aqueous solutions The Agnp-ACs also exhibited recyclability upto five, four, three and four cycles for Agnp-PSAC, Agnp-PSAC, Agnp-PCAC and Agnp-PAC respectively. The Agnp-PCAC also showed potential to act as SERS substrate for 4-NP.

3.6 References

Aditya, T., Pal, A., Pal, T., 2015. Nitroarene reduction: a trusted model reaction to test nanoparticle catalysts. Chem. Commun. 51, 9410–9431. doi:10.1039/C5CC01131K

Araujo, P.T., Mafra, D.L., Sato, K., Saito, R., Kong, J., Dresselhaus, M.S., 2012. Unraveling the interlayer-related phonon self-energy renormalization in bilayer graphene. Sci. Rep. 2, 1017. doi:10.1038/srep01017

Bhui, D.K., Misra, A., 2012. Synthesis of worm like silver nanoparticles in methyl cellulose polymeric matrix and its catalytic activity. Carbohydr. Polym. 89, 830–835. doi:http://dx.doi.org/10.1016/j.carbpol.2012.04.017

Cameron, D.S., Cooper, S.J., Dodgson, I.L., Harrison, B., Jenkins, J.W., 1990. Carbons as supports for precious metal catalysts. Catal. Today 7, 113–137. doi:http://dx.doi.org/10.1016/0920-5861(90)85012-D

Cañamares, M. V, Garcia-Ramos, J. V, Gómez-Varga, J.D., Domingo, C., Sanchez-Cortes, S., 2005. Comparative Study of the Morphology, Aggregation, Adherence to Glass, and Surface-Enhanced Raman Scattering Activity of Silver Nanoparticles Prepared by Chemical Reduction of Ag^+ Using Citrate and Hydroxylamine. Langmuir 21, 8546–8553. doi:10.1021/la050030l

Cançado, L.G., Jorio, A., Pimenta, M.A., 2007. Measuring the absolute Raman cross section of nanographites as a function of laser energy and crystallite size. Phys. Rev. B 76, 64304. doi:10.1103/PhysRevB.76.064304

Cárdenas-Lizana, F., Lamey, D., Perret, N., Gómez-Quero, S., Kiwi-Minsker, L., Keane, M.A., 2012. Au/Mo_2N as a new catalyst formulation for the hydrogenation of p-chloronitrobenzene in both liquid and gas phases. Catal. Commun. 21, 46–51. doi:http://dx.doi.org/10.1016/j.catcom.2012.01.027

Cárdenas-Lizana, F., Pedro, Z.M. De, Gómez-Quero, S., Kiwi-Minsker, L., Keane, M.A., 2015. Carbon supported gold and silver: Application in the gas phase hydrogenation of m-dinitrobenzene. J. Mol. Catal. A Chem. 408, 138–146.

doi:http://dx.doi.org/10.1016/j.molcata.2015.07.019

Chen, D., Qu, Z., Sun, Y., Gao, K., Wang, Y., 2013. Identification of reaction intermediates and mechanism responsible for highly active HCHO oxidation on Ag/MCM-41 catalysts. Appl. Catal. B Environ. 142–143, 838–848. doi:http://dx.doi.org/10.1016/j.apcatb.2013.06.025

Chen, Y., Wang, C., Liu, H., Qiu, J., Bao, X., 2005. Ag/SiO_2: a novel catalyst with high activity and selectivity for hydrogenation of chloronitrobenzenes. Chem. Commun. 5298–5300. doi:10.1039/B509595F

Chi, Y., Yuan, Q., Li, Y., Tu, J., Zhao, L., Li, N., Li, X., 2012. Synthesis of Fe_3O_4@SiO_2-Ag magnetic nanocomposite based on small-sized and highly dispersed silver nanoparticles for catalytic reduction of 4-nitrophenol. J. Colloid Interface Sci. 383, 96–102. doi:http://dx.doi.org/10.1016/j.jcis.2012.06.027

Choi, S., Jeong, Y., Yu, J., 2016. Spontaneous hydrolysis of borohydride required before its catalytic activation by metal nanoparticles. Catal. Commun. 84, 80–84. doi:http://dx.doi.org/10.1016/j.catcom.2016.06.008

Chusuei, C.C., Lai, X., Luo, K., Goodman, D.W., 2000. Modeling heterogeneous catalysts: metal clusters on planar oxide supports. Top. Catal. 14, 71–83. doi:10.1023/A:1009059100646

Coccia, F., Tonucci, L., Bosco, D., Bressan, M., d'Alessandro, N., 2012. One-pot synthesis of lignin-stabilised platinum and palladium nanoparticles and their catalytic behaviour in oxidation and reduction reactions. Green Chem. 14, 1073–1078. doi:10.1039/C2GC16524D

Cong, C., Yu, T., Saito, R., Dresselhaus, G.F., Dresselhaus, M.S., 2011. Second-Order Overtone and Combination Raman Modes of Graphene Layers in the Range of 1690−2150 cm−1. ACS Nano 5, 1600–1605. doi:10.1021/nn200010m

Couzi, M., Bruneel, J.-L., Talaga, D., Bokobza, L., 2016. A multi wavelength Raman scattering study of defective graphitic carbon materials: The first order Raman spectra revisited. Carbon N. Y. 107, 388–394.

doi:http://dx.doi.org/10.1016/j.carbon.2016.06.017

Crossley, M.L., 1922. The Chemistry of Intermediates. J. Ind. Eng. Chem. 14, 802–804. doi:10.1021/ie50153a023

Cuesta, A., Dhamelincourt, P., Laureyns, J., Martínez-Alonso, A., Tascón, J.M.D., 1994. Raman microprobe studies on carbon materials. Carbon N. Y. 32, 1523–1532. doi:http://dx.doi.org/10.1016/0008-6223(94)90148-1

Dong, Z., Le, X., Li, X., Zhang, W., Dong, C., Ma, J., 2014. Silver nanoparticles immobilized on fibrous nano-silica as highly efficient and recyclable heterogeneous catalyst for reduction of 4-nitrophenol and 2-nitroaniline. Appl. Catal. B Environ. 158–159, 129–135. doi:http://dx.doi.org/10.1016/j.apcatb.2014.04.015

Dotzauer, D.M., Bhattacharjee, S., Wen, Y., Bruening, M.L., 2009. Nanoparticle-Containing Membranes for the Catalytic Reduction of Nitroaromatic Compounds. Langmuir 25, 1865–1871. doi:10.1021/la803220z

Edison, T.J.I., Sethuraman, M.G., 2013. Biogenic robust synthesis of silver nanoparticles using Punica granatum peel and its application as a green catalyst for the reduction of an anthropogenic pollutant 4-nitrophenol. Spectrochim. Acta Part A Mol. Biomol. Spectrosc. 104, 262–264. doi:http://dx.doi.org/10.1016/j.saa.2012.11.084

Emmrich, M., 1999. Kinetics of the Alkaline Hydrolysis of 2,4,6-Trinitrotoluene in Aqueous Solution and Highly Contaminated Soils. Environ. Sci. Technol. 33, 3802–3805. doi:10.1021/es9903227

Esumi, K., Isono, R., Yoshimura, T., 2004. Preparation of PAMAM− and PPI−Metal (Silver, Platinum, and Palladium) Nanocomposites and Their Catalytic Activities for Reduction of 4-Nitrophenol. Langmuir 20, 237–243. doi:10.1021/la035440t

Ferrari, A.C., Meyer, J.C., Scardaci, V., Casiraghi, C., Lazzeri, M., Mauri, F., Piscanec, S., Jiang, D., Novoselov, K.S., Roth, S., Geim, A.K., 2006. Raman Spectrum of Graphene and Graphene Layers. Phys. Rev. Lett. 97, 187401.

doi:10.1103/PhysRevLett.97.187401

Ferrari, A.C., Robertson, J., 2000. Interpretation of Raman spectra of disordered and amorphous carbon. Phys. Rev. B 61, 14095–14107. doi:10.1103/PhysRevB.61.14095

Fonsaca, J.E.S., Elías, A.L., Domingues, S.H., Oliveira, M.M., Endo, M., Orth, E.S., Terrones, M., Zarbin, A.J.G., 2015. Graphene nanoribbons inducing cube-shaped Ag nanoparticle assemblies. Carbon N. Y. 93, 800–811. doi:http://dx.doi.org/10.1016/j.carbon.2015.05.098

Fortunati, E., D'Angelo, F., Martino, S., Orlacchio, A., Kenny, J.M., Armentano, I., 2011. Carbon nanotubes and silver nanoparticles for multifunctional conductive biopolymer composites. Carbon N. Y. 49, 2370–2379. doi:http://dx.doi.org/10.1016/j.carbon.2011.02.004

Fu, Y., Lu, Y., Polzer, F., Lux-Steiner, M.C., Fischer, C.-H., 2016. In-situ Synthesis of Stabilizer-Free Gold Nanocrystals with Controllable Shape on Substrates as Highly Active Catalysts for Multiple Use. Adv. Synth. Catal. 358, 1440–1448. doi:10.1002/adsc.201500848

Gao, S., Zhang, Z., Liu, K., Dong, B., 2016. Direct evidence of plasmonic enhancement on catalytic reduction of 4-nitrophenol over silver nanoparticles supported on flexible fibrous networks. Appl. Catal. B Environ. 188, 245–252. doi:http://dx.doi.org/10.1016/j.apcatb.2016.01.074

Guo, D.J., Li, H.L., 2005. Highly dispersed Ag nanoparticles on functional MWNT surfaces for methanol oxidation in alkaline solution. Carbon N. Y. 43, 1259–1264. doi:http://dx.doi.org/10.1016/j.carbon.2004.12.021

Hayakawa, K., Yoshimura, T., Esumi, K., 2003. Preparation of Gold−Dendrimer Nanocomposites by Laser Irradiation and Their Catalytic Reduction of 4-Nitrophenol. Langmuir 19, 5517–5521. doi:10.1021/la034339l

Hu, H., Xin, J.H., Hu, H., Wang, X., Miao, D., Liu, Y., 2015. Synthesis and stabilization of metal nanocatalysts for reduction reactions - a review. J. Mater.

Chem. A 3, 11157–11182. doi:10.1039/C5TA00753D

Huang, W.X., White, J.M., 2003. Revisiting NO_2 on Ag(1 1 1): a detailed TPD and RAIRS study. Surf. Sci. 529, 455–470. doi:http://dx.doi.org/10.1016/S0039-6028(03)00332-7

Huang, X., Xiao, Y., Zhang, W., Lang, M., 2012. In-situ formation of silver nanoparticles stabilized by amphiphilic star-shaped copolymer and their catalytic application. Appl. Surf. Sci. 258, 2655–2660. doi:http://dx.doi.org/10.1016/j.apsusc.2011.10.113

Ishida, T., Haruta, M., 2007. Gold Catalysts: Towards Sustainable Chemistry. Angew. Chemie Int. Ed. 46, 7154–7156. doi:10.1002/anie.200701622

Jawhari, T., Roid, A., Casado, J., 1995. Raman spectroscopic characterization of some commercially available carbon black materials. Carbon N. Y. 33, 1561–1565. doi:http://dx.doi.org/10.1016/0008-6223(95)00117-V

Ji, T., Chen, L., Mu, L., Yuan, R., Knoblauch, M., Bao, F.S., Zhu, J., 2016. In-situ reduction of Ag nanoparticles on oxygenated mesoporous carbon fabric: Exceptional catalyst for nitroaromatics reduction. Appl. Catal. B Environ. 182, 306–315. doi:http://dx.doi.org/10.1016/j.apcatb.2015.09.024

Jia, X., Ma, X., Wei, D., Dong, J., Qian, W., 2008. Direct formation of silver nanoparticles in cuttlebone-derived organic matrix for catalytic applications. Colloids Surfaces A Physicochem. Eng. Asp. 330, 234–240. doi:http://dx.doi.org/10.1016/j.colsurfa.2008.08.016

Jorio, A., Lucchese, M.M., Stavale, F., Achete, C.A., 2009. Raman spectroscopy study of Ar^+ bombardment in highly oriented pyrolytic graphite. Phys. status solidi 246, 2689–2692. doi:10.1002/pssb.200982314

Khalavka, Y., Becker, J., Sönnichsen, C., 2009. Synthesis of Rod-Shaped Gold Nanorattles with Improved Plasmon Sensitivity and Catalytic Activity. J. Am. Chem. Soc. 131, 1871–1875. doi:10.1021/ja806766w

Kleist, W., Pröckl, S.S., Drees, M., Köhler, K., Djakovitch, L., 2009. Amination of aryl chlorides and fluorides toward the synthesis of aromatic amines by palladium-catalyzed route or transition metal free way: Scopes and limitations. J. Mol. Catal. A Chem. 303, 15–22. doi:http://dx.doi.org/10.1016/j.molcata.2008.12.014

Ko, J.W., Li, J., Ko, W.B., 2015. Preparation of [C60]Fullerene Nanowhisker-gold Nanoparticle Composites and Reduction of 4-Nitrophenol through Catalysis. Nanomater. Nanotechnol. 1. doi:10.5772/62086

Kuroda, K., Ishida, T., Haruta, M., 2009. Reduction of 4-nitrophenol to 4-aminophenol over Au nanoparticles deposited on PMMA. J. Mol. Catal. A Chem. 298, 7–11. doi:http://dx.doi.org/10.1016/j.molcata.2008.09.009

Lam, E., Hrapovic, S., Majid, E., Chong, J.H., Luong, J.H.T., 2012. Catalysis using gold nanoparticles decorated on nanocrystalline cellulose. Nanoscale 4, 997–1002. doi:10.1039/C2NR11558A

Larouche, N., Stansfield, B.L., 2010. Classifying nanostructured carbons using graphitic indices derived from Raman spectra. Carbon N. Y. 48, 620–629. doi:http://dx.doi.org/10.1016/j.carbon.2009.10.002

Lee, H.S., Kim, J.E., Kim, T., Suh, K.S., 2015. Ionic liquid-assisted synthesis of highly branched Ag:AgCl hybrids and their photocatalytic activity. J. Alloys Compd. 621, 378–382. doi:http://dx.doi.org/10.1016/j.jallcom.2014.09.222

Leelavathi, A., Bhaskara Rao, T.U., Pradeep, T., 2011. Supported quantum clusters of silver as enhanced catalysts for reduction. Nanoscale Res. Lett. doi:10.1186/1556-276X-6-123

Li, J., Liu, C., Liu, Y., 2012. Au/graphene hydrogel: synthesis, characterization and its use for catalytic reduction of 4-nitrophenol. J. Mater. Chem. 22, 8426–8430. doi:10.1039/C2JM16386A

Li, X., Wang, X., Song, S., Liu, D., Zhang, H., 2012. Selectively deposited noble metal nanoparticles on Fe_3O_4/graphene composites: stable, recyclable, and

magnetically separable catalysts. Chemistry 18, 7601–7607. doi:10.1002/chem.201103726

Liang, G.D., Bao, S.P., Tjong, S.C., 2007. Microstructure and properties of polypropylene composites filled with silver and carbon nanotube nanoparticles prepared by melt-compounding. Mater. Sci. Eng. B 142, 55–61. doi:http://dx.doi.org/10.1016/j.mseb.2007.06.028

Lin, F., Doong, R., 2011. Bifunctional Au-Fe_3O_4 Heterostructures for Magnetically Recyclable Catalysis of Nitrophenol Reduction. J. Phys. Chem. C 115, 6591–6598. doi:10.1021/jp110956k

Liu, P., Zhao, M., 2009. Silver nanoparticle supported on halloysite nanotubes catalyzed reduction of 4-nitrophenol (4-NP). Appl. Surf. Sci. 255, 3989–3993. doi:http://dx.doi.org/10.1016/j.apsusc.2008.10.094

Liu, R., Gao, N., Zhen, F., Zhang, Y., Mei, L., Zeng, X., 2013. Doping effect of Al_2O_3 and CeO_2 on Fe_2O_3 support for gold catalyst in CO oxidation at low-temperature. Chem. Eng. J. 225, 245–253. doi:http://dx.doi.org/10.1016/j.cej.2013.03.118

Liu, X., Cheng, H., Cui, P., 2014. Catalysis by silver nanoparticles/porous silicon for the reduction of nitroaromatics in the presence of sodium borohydride. Appl. Surf. Sci. 292, 695–701. doi:http://dx.doi.org/10.1016/j.apsusc.2013.12.036

Liu, X., Jin, R., Chen, D., Chen, L., Xing, S., Xing, H., Xing, Y., Su, Z., 2015. In situ assembly of monodispersed Ag nanoparticles in the channels of ordered mesopolymers as a highly active and reusable hydrogenation catalyst. J. Mater. Chem. A 3, 4307–4313. doi:10.1039/C4TA06049K

Liu, Y., Liu, X., Wang, X., 2010. Biomimetic Synthesis of Gelatin Polypeptide-Assisted Noble-Metal Nanoparticles and Their Interaction Study. Nanoscale Res Lett 6, 22. doi:10.1007/s11671-010-9756-1

Lu, Y., Mei, Y., Schrinner, M., Ballauff, M., Möller, M.W., Breu, J., 2007. In Situ Formation of Ag Nanoparticles in Spherical Polyacrylic Acid Brushes by UV

Irradiation. J. Phys. Chem. C 111, 7676–7681. doi:10.1021/jp070973m

Lucchese, M.M., Stavale, F., Ferreira, E.H.M., Vilani, C., Moutinho, M.V.O., Capaz, R.B., Achete, C.A., Jorio, A., 2010. Quantifying ion-induced defects and Raman relaxation length in graphene. Carbon N. Y. 48, 1592–1597. doi:http://dx.doi.org/10.1016/j.carbon.2009.12.057

Mäkinen, A.E., Nissilä, M.E., Puhakka, J.A., 2012. Dark fermentative hydrogen production from xylose by a hot spring enrichment culture. Int. J. Hydrogen Energy 37, 12234–12240. doi:http://dx.doi.org/10.1016/j.ijhydene.2012.05.158

Mallick, K., Witcomb, M.J., Scurrell, M.S., 2004. Polymer stabilized silver nanoparticles: A photochemical synthesis route. J. Mater. Sci. 39, 4459–4463. doi:10.1023/B:JMSC.0000034138.80116.50

Manivannan, S., Krishnakumari, B., Ramaraj, R., 2012. Synthesis of silicate sol–gel matrix embedded silver nanostructures: Efficient nanocatalyst for the reduction of 4-nitrophenol. Chem. Eng. J. 204–206, 16–22. doi:http://dx.doi.org/10.1016/j.cej.2012.07.092

Mao, Q., Shi, S., Wang, H., 2015. Biomimetic Nanowire Structured Hydrogels as Highly Active and Recyclable Catalyst Carriers. ACS Sustain. Chem. Eng. 3, 1915–1924. doi:10.1021/acssuschemeng.5b00482

Marín, A., Barbas, C., 2004. LC/MS for the degradation profiling of cough–cold products under forced conditions. J. Pharm. Biomed. Anal. 35, 1035–1045. doi:http://dx.doi.org/10.1016/j.jpba.2004.03.011

Mbhele, Z.H., Salemane, M.G., van Sittert, C.G.C.E., Nedeljković, J.M., Djoković, V., Luyt, A.S., 2003. Fabrication and Characterization of Silver−Polyvinyl Alcohol Nanocomposites. Chem. Mater. 15, 5019–5024. doi:10.1021/cm034505a

Mehl, H., Oliveira, M.M., Zarbin, A.J.G., 2015. Thin and transparent films of graphene/silver nanoparticles obtained at liquid–liquid interfaces: Preparation, characterization and application as SERS substrates. J. Colloid Interface Sci.

438, 29–38. doi:http://dx.doi.org/10.1016/j.jcis.2014.09.068

Mei, Y., Sharma, G., Lu, Y., Ballauff, M., Drechsler, M., Irrgang, T., Kempe, R., 2005. High Catalytic Activity of Platinum Nanoparticles Immobilized on Spherical Polyelectrolyte Brushes. Langmuir 21, 12229–12234. doi:10.1021/la052120w

Mesmer, R.E., Jolly, W.L., 1962. The Hydrolysis of Aqueous Hydroborate. Inorg. Chem. 1, 608–612. doi:10.1021/ic50003a031

Mohammed, M.K.A., Al-Mousoi, A.K., Khalaf, H.A., 2016. Deposition of multi-layer graphene (MLG) film on glass slide by flame synthesis technique. Opt. - Int. J. Light Electron Opt. 127, 9848–9852. doi:http://dx.doi.org/10.1016/j.ijleo.2016.07.043

Mohring, R.M., Cantave, R., Fennimore, K.A., McNamara, K.., 2009. Methods and devices for hydrogen generation, US 20090104481 A1.

Mondal, K., Kumar, J., Sharma, A., 2013. Self-organized macroporous thin carbon films for supported metal catalysis. Colloids Surfaces A Physicochem. Eng. Asp. 427, 83–94. doi:http://dx.doi.org/10.1016/j.colsurfa.2013.03.024

Mori, K., Kumami, A., Tomonari, M., Yamashita, H., 2009. A pH-Induced Size Controlled Deposition of Colloidal Ag Nanoparticles on Alumina Support for Catalytic Application. J. Phys. Chem. C 113, 16850–16854. doi:10.1021/jp907277g

Murugadoss, A., Chattopadhyay, A., 2008. A “green” chitosan–silver nanoparticle composite as a heterogeneous as well as micro-heterogeneous catalyst. Nanotechnology 19, 15603.

Murugan, E., Jebaranjitham, J.N., 2012. Synthesis and characterization of silver nanoparticles supported on surface-modified poly(N-vinylimidazale) as catalysts for the reduction of 4-nitrophenol. J. Mol. Catal. A Chem. 365, 128–135. doi:http://dx.doi.org/10.1016/j.molcata.2012.08.021

Nadagouda, M.N., Speth, T.F., Varma, R.S., 2011. Microwave-Assisted Green Synthesis of Silver Nanostructures. Acc. Chem. Res. 44, 469–478. doi:10.1021/ar1001457

Naik, B., Hazra, S., Muktesh, P., Prasad, V.S.., Ghosh, N.N., 2011. A Facile Method for Preparation of Ag Nanoparticle Loaded MCM-41 and Study of Its Catalytic Activity for Reduction of 4-Nitrophenol. Sci. Adv. Mater. 3, 1025–1030.

Naik, B., Hazra, S., Prasad, V.S., Ghosh, N.N., 2011. Synthesis of Ag nanoparticles within the pores of SBA-15: An efficient catalyst for reduction of 4-nitrophenol. Catal. Commun. 12, 1104–1108. doi:http://dx.doi.org/10.1016/j.catcom.2011.03.028

Naik, B., Prasad, V.S., Ghosh, N.N., 2012. Preparation of Ag nanoparticle loaded mesoporous γ-alumina catalyst and its catalytic activity for reduction of 4-nitrophenol. Powder Technol. 232, 1–6. doi:http://dx.doi.org/10.1016/j.powtec.2012.07.052

Nandanwar, S.U., Chakraborty, M., 2012. Synthesis of Colloidal CuO/γ-Al_2O_3 by Microemulsion and Its Catalytic Reduction of Aromatic Nitro Compounds. Chinese J. Catal. 33, 1532–1541. doi:http://dx.doi.org/10.1016/S1872-2067(11)60433-6

Nasrollahzadeh, M., Atarod, M., Jaleh, B., Gandomirouzbahani, M., 2016. In situ green synthesis of Ag nanoparticles on graphene oxide/TiO_2 nanocomposite and their catalytic activity for the reduction of 4-nitrophenol, congo red and methylene blue. Ceram. Int. 42, 8587–8596. doi:http://dx.doi.org/10.1016/j.ceramint.2016.02.088

Niilisk, A., Kozlova, J., Alles, H., Aarik, J., Sammelselg, V., 2016. Raman characterization of stacking in multi-layer graphene grown on Ni. Carbon N. Y. 98, 658–665. doi:http://dx.doi.org/10.1016/j.carbon.2015.11.050

Patel, A.C., Li, S., Wang, C., Zhang, W., Wei, Y., 2007. Electrospinning of Porous Silica Nanofibers Containing Silver Nanoparticles for Catalytic Applications. Chem. Mater. 19, 1231–1238. doi:10.1021/cm061331z

Patil, N.S., Jha, R., Uphade, B.S., Bhargava, S.K., Choudhary, V.R., 2004. Epoxidation of styrene by anhydrous t-butyl hydroperoxide over gold supported on Al_2O_3, Ga_2O_3, In_2O_3 and Tl_2O_3. Appl. Catal. A Gen. 275, 87–93. doi:http://dx.doi.org/10.1016/j.apcata.2004.07.023

Patterson, H.H., Gomez, R.S., Lu, H., Yson, R.L., 2007. Nanoclusters of silver doped in zeolites as photocatalysts. Catal. Today 120, 168–173. doi:http://dx.doi.org/10.1016/j.cattod.2006.07.057

Peláez, R.J., Castelo, A., Afonso, C.N., Borrás, A., Espinós, J.P., Riedel, S., Leiderer, P., Boneberg, J., 2013. Enhanced reactivity and related optical changes of Ag nanoparticles on amorphous Al_2O_3 supports. Nanotechnology 24, 365702.

Pozun, Z.D., Rodenbusch, S.E., Keller, E., Tran, K., Tang, W., Stevenson, K.J., Henkelman, G., 2013. A Systematic Investigation of p-Nitrophenol Reduction by Bimetallic Dendrimer Encapsulated Nanoparticles. J. Phys. Chem. C 117, 7598–7604. doi:10.1021/jp312588u

Pradhan, N., Pal, A., Pal, T., 2002. Silver nanoparticle catalyzed reduction of aromatic nitro compounds. Colloids Surfaces A Physicochem. Eng. Asp. 196, 247–257. doi:http://dx.doi.org/10.1016/S0927-7757(01)01040-8

Praharaj, S., Nath, S., Ghosh, S.K., Kundu, S., Pal, T., 2004. Immobilization and recovery of au nanoparticles from anion exchange resin: resin-bound nanoparticle matrix as a catalyst for the reduction of 4-nitrophenol. Langmuir 20, 9889–9892. doi:10.1021/la0486281

Rajagopal, S., Spatola, A.F., 1995. Mechanism of Palladium-Catalyzed Transfer Hydrogenolysis of Aryl Chlorides by Formate Salts. J. Org. Chem. 60, 1347–1355. doi:10.1021/jo00110a045

Rajesh, R., Venkatesan, R., 2012. Encapsulation of silver nanoparticles into graphite grafted with hyperbranched poly(amidoamine) dendrimer and their catalytic activity towards reduction of nitro aromatics. J. Mol. Catal. A Chem. 359, 88–96. doi:http://dx.doi.org/10.1016/j.molcata.2012.04.001

Rao, R., Podila, R., Tsuchikawa, R., Katoch, J., Tishler, D., Rao, A.M., Ishigami, M., 2011. Effects of Layer Stacking on the Combination Raman Modes in Graphene. ACS Nano 5, 1594–1599. doi:10.1021/nn1031017

Rashid, M.H., Mandal, T.K., 2007. Synthesis and Catalytic Application of Nanostructured Silver Dendrites. J. Phys. Chem. C 111, 16750–16760. doi:10.1021/jp074963x

Rodríguez-reinoso, F., 1998. The role of carbon materials in heterogeneous catalysis. Carbon N. Y. 36, 159–175.

doi:http://dx.doi.org/10.1016/S0008-6223(97)00173-5

Russo, M., Armetta, F., Riela, S., Martino, D.C., Meo, P. Lo, Noto, R., 2015. Silver nanoparticles stabilized by a polyaminocyclodextrin as catalysts for the reduction of nitroaromatic compounds. J. Mol. Catal. A Chem. 408, 250–261. doi:http://dx.doi.org/10.1016/j.molcata.2015.07.031

Saha, S., Pal, A., Kundu, S., Basu, S., Pal, T., 2010. Photochemical Green Synthesis of Calcium-Alginate-Stabilized Ag and Au Nanoparticles and Their Catalytic Application to 4-Nitrophenol Reduction. Langmuir 26, 2885–2893. doi:10.1021/la902950x

Santos, K. de O., Elias, W.C., Signori, A.M., Giacomelli, F.C., Yang, H., Domingos, J.B., 2012. Synthesis and Catalytic Properties of Silver Nanoparticle–Linear Polyethylene Imine Colloidal Systems. J. Phys. Chem. C 116, 4594–4604. doi:10.1021/jp2087169

Sato, K., Park, J.S., Saito, R., Cong, C., Yu, T., Lui, C.H., Heinz, T.F., Dresselhaus, G., Dresselhaus, M.S., 2011. Raman spectra of out-of-plane phonons in bilayer graphene. Phys. Rev. B 84, 35419. doi:10.1103/PhysRevB.84.035419

Selvakannan, P.R., Mantri, K., Tardio, J., Bhargava, S.K., 2013. High surface area Au–SBA-15 and Au–MCM-41 materials synthesis: Tryptophan amino acid mediated confinement of gold nanostructures within the mesoporous silica pore walls. J. Colloid Interface Sci. 394, 475–484.

doi:http://dx.doi.org/10.1016/j.jcis.2012.12.008

Shimizu, K., Miyamoto, Y., Satsuma, A., 2010. Size- and support-dependent silver cluster catalysis for chemoselective hydrogenation of nitroaromatics. J. Catal. 270, 86–94. doi:http://dx.doi.org/10.1016/j.jcat.2009.12.009

Shimizu, K., Shimura, K., Nishimura, M., Satsuma, A., 2011. Direct Synthesis of N-Substituted Anilines from Nitroaromatics and Alcohols under H_2 by Alumina-Supported Silver Cluster Catalysts. ChemCatChem 3, 1755–1758. doi:10.1002/cctc.201100171

Shin, K.S., Choi, J.-Y., Park, C.S., Jang, H.J., Kim, K., 2009. Facile Synthesis and Catalytic Application of Silver-Deposited Magnetic Nanoparticles. Catal. Letters 133, 1. doi:10.1007/s10562-009-0124-7

Shurtless, J.K., Patton, J.M., Ladd, E.., 2009. Apparatus, System, And Method For Promoting A Substantially Complete Reaction of An Anhydrous Hydride Reactant, US 8357213 B2.

Solís-López, M., Durán-Moreno, A., Rigas, F., Morales, A.A., Navarrete, M., Ramírez-Zamora, R.M., 2014. 9 - Assessment of Copper Slag as a Sustainable Fenton-Type Photocatalyst for Water Disinfection, in: Ahuja, S. (Ed.), Water Reclamation and Sustainability. Elsevier, Boston, pp. 199–227. doi:http://dx.doi.org/10.1016/B978-0-12-411645-0.00009-2

Sreekanth, T.V.M., Jung, M.-J., Eom, I.-Y., 2016. Green synthesis of silver nanoparticles, decorated on graphene oxide nanosheets and their catalytic activity. Appl. Surf. Sci. 361, 102–106. doi:http://dx.doi.org/10.1016/j.apsusc.2015.11.146

Tajbakhsh, M., Alinezhad, H., Nasrollahzadeh, M., Kamali, T.A., 2016. Green synthesis of the Ag/HZSM-5 nanocomposite by using Euphorbia heterophylla leaf extract: A recoverable catalyst for reduction of organic dyes. J. Alloys Compd. 685, 258–265. doi:http://dx.doi.org/10.1016/j.jallcom.2016.05.278

Vats, T., Dutt, S., Kumar, R., Siril, P.F., 2016. Facile synthesis of pristine graphene-

palladium nanocomposites with extraordinary catalytic activities using swollen liquid crystals. Sci. Rep. 6, 33053.

Venezia, A.M., Murania, R., Parola, V. La, Pawelec, B., Fierro, J.L.G., 2010. Post-synthesis alumination of MCM-41: Effect of the acidity on the HDS activity of supported Pd catalysts. Appl. Catal. A Gen. 383, 211–216. doi:http://dx.doi.org/10.1016/j.apcata.2010.06.001

Voronov, O.A., Jr., K.W.S., 2010. Raman scattering in a new carbon material. Diam. Relat. Mater. 19, 31–39. doi:http://dx.doi.org/10.1016/j.diamond.2009.10.018

Wepasnick, K.A., Smith, B.A., Schrote, K.E., Wilson, H.K., Diegelmann, S.R., Fairbrother, D.H., 2011. Surface and structural characterization of multi-walled carbon nanotubes following different oxidative treatments. Carbon N. Y. 49, 24–36. doi:http://dx.doi.org/10.1016/j.carbon.2010.08.034

Wu, Z., Mao, X., Zi, Q., Zhang, R., Dou, T., Yip, A.C.K., 2014. Mechanism and kinetics of sodium borohydride hydrolysis over crystalline nickel and nickel boride and amorphous nickel–boron nanoparticles. J. Power Sources 268, 596–603. doi:http://dx.doi.org/10.1016/j.jpowsour.2014.06.067

Wunder, S., Polzer, F., Lu, Y., Mei, Y., Ballauff, M., 2010. Kinetic Analysis of Catalytic Reduction of 4-Nitrophenol by Metallic Nanoparticles Immobilized in Spherical Polyelectrolyte Brushes. J. Phys. Chem. C 114, 8814–8820. doi:10.1021/jp101125j

Xiong, Y., Luo, G., Chen, C., Yuan, H., Shen, Q., Li, M., 2012. In situ synthesis of zero-valent silver nanoparticles in polymethylmethacrylate under high temperature. Appl. Surf. Sci. 258, 5822–5826. doi:http://dx.doi.org/10.1016/j.apsusc.2012.02.108

Yang, X.-F., Wang, A., Qiao, B., Li, J., Liu, J., Zhang, T., 2013. Single-Atom Catalysts: A New Frontier in Heterogeneous Catalysis. Acc. Chem. Res. 46, 1740–1748. doi:10.1021/ar300361m

Zarejousheghani, M., Möder, M., Borsdorf, H., 2013. A new strategy for synthesis of

an in-tube molecularly imprinted polymer-solid phase microextraction device: Selective off-line extraction of 4-nitrophenol as an example of priority pollutants from environmental water samples. Anal. Chim. Acta 798, 48–55. doi:http://dx.doi.org/10.1016/j.aca.2013.08.038

Zhang, C.-L., Yu, S.-H., 2014. Nanoparticles meet electrospinning: recent advances and future prospects. Chem. Soc. Rev. 43, 4423–4448. doi:10.1039/C3CS60426H

Zhang, J., Chen, G., Chaker, M., Rosei, F., Ma, D., 2013. Gold nanoparticle decorated ceria nanotubes with significantly high catalytic activity for the reduction of nitrophenol and mechanism study. Appl. Catal. B Environ. 132–133, 107–115. doi:http://dx.doi.org/10.1016/j.apcatb.2012.11.030

Zhang, P., Shao, C., Zhang, Z., Zhang, M., Mu, J., Guo, Z., Liu, Y., 2011. In situ assembly of well-dispersed Ag nanoparticles (AgNPs) on electrospun carbon nanofibers (CNFs) for catalytic reduction of 4-nitrophenol. Nanoscale 3, 3357–3363. doi:10.1039/C1NR10405E

Zhang, X., Qu, Z., Yu, F., Wang, Y., 2013. High-temperature diffusion induced high activity of SBA-15 supported Ag particles for low temperature CO oxidation at room temperature. J. Catal. 297, 264–271. doi:http://dx.doi.org/10.1016/j.jcat.2012.10.019

Zhang, Z., Han, M., 2003. One-step preparation of size-selected and well-dispersed silver nanocrystals in polyacrylonitrile by simultaneous reduction and polymerization. J. Mater. Chem. 13, 641–643. doi:10.1039/B212428A

Zhang, Z., Shao, C., Sun, Y., Mu, J., Zhang, M., Zhang, P., Guo, Z., Liang, P., Wang, C., Liu, Y., 2012. Tubular nanocomposite catalysts based on size-controlled and highly dispersed silver nanoparticles assembled on electrospun silica nanotubes for catalytic reduction of 4-nitrophenol. J. Mater. Chem. 22, 1387–1395. doi:10.1039/C1JM13421C

Zhang, Z., Shao, C., Zou, P., Zhang, P., Zhang, M., Mu, J., Guo, Z., Li, X., Wang, C., Liu, Y., 2011. In situ assembly of well-dispersed gold nanoparticles on

electrospun silica nanotubes for catalytic reduction of 4-nitrophenol. Chem. Commun. 47, 3906–3908. doi:10.1039/C0CC05693F

Zheng, J., Lin, H., Wang, Y., Zheng, X., Duan, X., Yuan, Y., 2013. Efficient low-temperature selective hydrogenation of esters on bimetallic Au–Ag/SBA-15 catalyst. J. Catal. 297, 110–118. doi:http://dx.doi.org/10.1016/j.jcat.2012.09.023

Zheng, Y., Shu, J., Wang, Z., 2015. AgCl@Ag composites with rough surfaces as bifunctional catalyst for the photooxidation and catalytic reduction of 4-nitrophenol. Mater. Lett. 158, 339–342. doi:http://dx.doi.org/10.1016/j.matlet.2015.06.033

Zhu, G.-H., Xiang, X.-D., Melman, J., 2007. Hydrogen generator solid fuel cartridge, US 20070271844.

Zhu, M., Wang, C., Meng, D., Diao, G., 2013. In situ synthesis of silver nanostructures on magnetic Fe_3O_4@C core-shell nanocomposites and their application in catalytic reduction reactions. J. Mater. Chem. A 1, 2118–2125. doi:10.1039/C2TA00669C